

# Core-Collapse Supernovae in Binaries as the Origin of Galactic Hyper-Runaway Stars

F. A. Evans<sup>1\*</sup>, M. Renzo<sup>2</sup>, E. M. Rossi<sup>1</sup>

<sup>1</sup>*Leiden Observatory, Leiden University, PO Box 9513, NL-2300 RA Leiden, The Netherlands*

<sup>2</sup>*Center for Computational Astrophysics, Flatiron Institute, 162 5th Ave., New York, NY 10010 USA*

Accepted XXX. Received YYY; in original form ZZZ

## ABSTRACT

Several stars detected moving at velocities near to or exceeding the Galactic escape speed likely originated in the Milky Way disc. We quantitatively explore the ‘binary supernova scenario’ hypothesis, wherein these ‘hyper-runaway’ stars are ejected at large peculiar velocities when their close, massive binary companions undergo a core-collapse supernova and the binary is disrupted. We perform an extensive suite of binary population synthesis simulations evolving massive systems to determine the assumptions and parameters which most impact the ejection rate of fast stars. In a simulation tailored to eject fast stars, we find the most likely hyper-runaway star progenitor binary is composed of a massive ( $\sim 30 M_{\odot}$ ) primary and a  $\sim 3 - 4 M_{\odot}$  companion on an orbital period that shrinks to  $\lesssim 1$  day prior to the core collapse following a common envelope phase. The black hole remnant formed from the primary must receive a natal kick  $\gtrsim 1000 \text{ km s}^{-1}$  to disrupt the binary and eject the companion at a large velocity. We compare the fast stars produced in these simulations to a contemporary census of early-type Milky Way hyper-runaway star candidates. We find that these rare objects may be produced in sufficient number only when poorly-constrained binary evolution parameters related to the strength of post-core collapse remnant natal kicks and common envelope efficiency are adjusted to values currently unsupported – but not excluded – by the literature. We discuss observational implications that may constrain the existence of these putative progenitor systems.

**Key words:** stars: kinematics and dynamics, massive – supernovae: general – binaries: general

## 1 INTRODUCTION

In recent years, works have reported with an increasing frequency detections of early-type main sequence (MS) stars in the Galactic halo moving at very high velocities, near to or exceeding the Galactic escape velocity at their position (e.g., Brown et al. 2005; Hirsch et al. 2005; Edelmann et al. 2005; Brown et al. 2006, 2009, 2012, 2014; Zhong et al. 2014; Huang et al. 2017; Irrgang et al. 2019; Koposov et al. 2019, and references therein). For reference, the Galactic escape velocity in the Solar Neighbourhood is  $\sim 530 \text{ km s}^{-1}$  (Piffl et al. 2014; Williams et al. 2017) and falls to  $\lesssim 400 \text{ km s}^{-1}$  beyond 50 kpc from the centre of the Milky Way (Williams et al. 2017). The population of high velocity stars is increasing further in the *Gaia* era (Gaia Collaboration et al. 2016, 2018), with the European Space Agency satellite providing precise astrometry for billions of Milky Way sources. The

short-lived nature of early-type stars and the dearth of star formation in the Galactic stellar halo suggest that these fast stars were not likely formed in-situ in the halo; rather, they were likely accelerated and ejected from their primal birthplaces. They therefore flag extreme astrophysical and dynamical processes occurring in the Milky Way. These processes as well as the uncertain initial conditions and physics governing them can be elucidated by studying the properties and kinematics of these fast-moving stars. See Brown (2015) for a recent review on these objects.

There exist a number of mechanisms to accelerate stars to such extreme velocities. Hills (1988) predicted that tight stellar binaries in the Galactic Centre (GC) could be tidally disrupted by a supermassive black hole (SMBH) lurking in the centre of the Milky Way. One member of the binary is captured in orbit around the SMBH while its companion is ejected with a very high velocity,  $\sim 1000 \text{ km s}^{-1}$ , giving rise to a population of so-called ‘hyper-velocity stars’ (HVS). Variations on this mechanism include the interaction of a

\* E-mail: evans@strw.leidenuniv.nl

single star with a binary system consisting of two SMBHs or a SMBH and an intermediate mass black hole (e.g. Yu & Tremaine 2003; Gualandris et al. 2005; Sesana et al. 2006; Guillochon & Loeb 2015), or the disruption of a globular cluster by a single SMBH or binary massive black hole pair in the GC (Capuzzo-Dolcetta & Fragione 2015; Fragione & Capuzzo-Dolcetta 2016). Regardless, a GC origin for hyper-velocity stars is a shared element of the above mechanisms. Theoretical estimates place the HVS ejection rate from the GC on the order of  $10^{-4} \text{ yr}^{-1}$  (Hills 1988; Perets et al. 2007; Zhang et al. 2013).

With perhaps the notable exception of S5-HVS1 (Koposov et al. 2019), the GC cannot be identified indisputably as the origin of many HVS candidates with contemporary astrometric measurements. However, especially given the high-precision astrometry provided by the second data release (DR2) of the *Gaia* mission (Gaia Collaboration et al. 2016, 2018), the GC can be ruled out as the spatial origin of many HVS candidates (see e.g. Irrgang et al. 2018). Other mechanisms must therefore be invoked to explain the extreme velocity of these stars. While tidal disruption of infalling dwarf galaxies (Abadi et al. 2009) or ejection from the Large Magellanic Cloud (Przybilla et al. 2008a; Boubert & Evans 2016; Boubert et al. 2017; Lennon et al. 2017; Erkal et al. 2019) or M31 (Sherwin et al. 2008) can explain extreme velocity stars whose past trajectories seem to point towards extragalactic space, the most plausible origin for many high velocity star candidates seems to be the Milky Way disc (e.g., Heber et al. 2008b; Silva & Napiwotzki 2011; Palladino et al. 2014; Irrgang et al. 2018, 2019; Marchetti et al. 2019). This is in spite of the fact that theoretical studies predict GC-ejected high-velocity stars to far outnumber disc-ejected high-velocity stars (Bromley et al. 2009; Kenyon et al. 2014).

A number of processes can be invoked to explain the existence of these disc-ejected high velocity stars. In a tight white dwarf/helium star binary, the deposition of a critical amount of helium onto the accreting white dwarf can result in the thermonuclear detonation of the white dwarf – a proposed progenitor for Type Ia supernovae (e.g. Wang et al. 2009; Justham et al. 2009). The donor star can be ejected at a velocity unbound to the Milky Way and therefore be observed as a hyper-velocity helium star or (eventually) a hyper-velocity white dwarf (Hansen 2003; Wang & Han 2009; Geier et al. 2013, 2015; Bauer et al. 2019; Neunteufel 2020). Surviving white dwarf donor companions can also be ejected at extreme velocities in the dynamically-driven double-degenerate double detonation Type Ia supernovae scenario (D<sup>6</sup>; Shen et al. 2018).

For *main sequence* high-velocity stars seemingly ejected from the Galactic disc, on the other hand, two main processes are typically blamed. In the dynamical ejection scenario (DES, e.g. Poveda et al. 1967; Leonard & Duncan 1990; Leonard 1991; Perets & Šubr 2012; Oh & Kroupa 2016), exchange encounters in dense stellar systems (Aarseth 1974) may eject stars at high velocities. In the binary supernova scenario (BSS; e.g. Blaauw 1961; Boersma 1961; Tauris & Takens 1998; Portegies Zwart 2000; Tauris 2015; Renzo et al. 2019b), the massive primary in a binary system explodes in a core-collapse (CC) supernova, disrupting the binary and ejecting its main-sequence companion with a velocity comparable to its pre-CC orbital velocity. Both processes are

known to occur in the Milky Way (Hoogerwerf et al. 2001; Jilinski et al. 2010) and are generally thought to be responsible for the known sample of ‘runaway stars’ with ejection velocities  $\geq 30 - 40 \text{ km s}^{-1}$  (Blaauw 1961), though their relative contribution is not yet well-constrained (see Hoogerwerf et al. 2001; Renzo et al. 2019b). With characteristic ejection speeds on the order of a few tens of  $\text{km s}^{-1}$ , it is not yet known whether these mechanisms can eject stars on the order of hundreds of  $\text{km s}^{-1}$  with sufficient frequency to explain the current known sample of ‘hyper-runaway stars’ (HRSs) – runaway stars ejected near to or above the Galactic escape velocity at their location. While ejection velocities in the neighbourhood of  $\sim 1000 \text{ km s}^{-1}$  are possible in both the DES (Leonard 1991) and BSS (e.g., Tauris & Takens 1998; Tauris 2015) scenarios, these situations are thought to be rare. Recent N-body simulations of young star clusters have found that ejections in excess  $200 \text{ km s}^{-1}$  are very rare (Perets & Šubr 2012; Oh & Kroupa 2016). Binary population synthesis models simulating a large number of binary systems show that ejections above  $200 \text{ km s}^{-1}$  are vastly outnumbered by ejections on the order of  $\sim 10 \text{ km s}^{-1}$  (Portegies Zwart 2000; Eldridge et al. 2011; Renzo et al. 2019b).

Extreme velocity stars are interesting beyond their status as astrophysical oddities – the violent and uncertain physical processes that generate them leave an imprint on their kinematics and properties. The population of stars ejected via the BSS and their mass and velocity distributions provide constraints on many uncertain parameters governing binary evolution and core-collapse supernovae – in particular the debated physics of the common envelope phase and the nature of the natal ‘kicks’ imparted on compact objects produced following CC events. Stars ejected via the DES can reveal information about the initial conditions describing their parent clusters. Genuine hyper-velocity stars ejected from the GC offer a convenient ‘back door’ into studying the dust-obscured and source-crowded GC environment (e.g., Zhang et al. 2013; Madigan et al. 2014; Rossi et al. 2017), in particular the origin and nature of the Milky Way’s nuclear star cluster (see Böker 2010, for a review), the interplay between Sgr A\* and its environment (see Genzel et al. 2010, for a review), and the growth of Sgr A\* via tidal disruption of former HVS companions (Bromley et al. 2012). The long journey from GC to outer halo makes GC-ejected hyper-velocity stars intriguing dynamical tracers for studying the size, mass and shape of the Galactic dark matter halo (e.g., Gnedin et al. 2005; Yu & Madau 2007; Kenyon et al. 2008, 2014; Rossi et al. 2017; Contigiani et al. 2019).

In this paper, we focus on HRSs ejected following a core-collapse event occurring in a massive binary system, building on the recent work of Renzo et al. (2019b), hereafter R19. They use a rapid binary population synthesis code to examine the kinematic signatures of ejected stars. To account for uncertainties in the initial conditions and physical processes important for binary evolution, they ran an extensive grid of simulations varying relevant assumptions. This allowed them to i) make concrete observational predictions by showing which aspects of the kinematic signatures are robust to model variations and ii) identify which assumptions and processes most strongly impact the kinematic observables, so that they may be constrained by future observations. They find in general across all model variations that the majority of binaries disrupted following the CC of the

primary eject slow-moving ‘walkaway stars’ ( $v \lesssim 30 \text{ km s}^{-1}$ ), a term first introduced in [de Mink et al. \(2012\)](#). They also find, however, that the absolute number of ejected companions and their velocity distribution depend intimately on assumptions about the natal kick delivered to remnant neutron stars (NSs) and black holes (BHs) due to asymmetries in the supernova explosion. While high-velocity ejections were not the main focus of the work, [R19](#) remark on the presence of a minor peak in the ejection velocity distribution in the vicinity of  $100 \text{ km s}^{-1} \lesssim v \lesssim 400 \text{ km s}^{-1}$  (c.f. Fig. C.2 in [R19](#)), resulting from binaries which experienced a common envelope phase without significant accretion by the secondary.

In this work we employ the same simulation framework and approach as [R19](#) to focus further on these fastest ejections: we study whether the BSS is able to eject fast stars with sufficient frequency to match the current sample of identified HRS candidates in the Milky Way. We vary relevant uncertain physical parameters and determine which most strongly affect the likelihood of a system ejecting a companion at a very high velocity.

This paper is organized as follows. In Sec. 2 we describe our binary population synthesis code, the physical assumptions we use in all our models and how we compare the simulation results to current HRS candidates. In Sec. 3 we outline how we build and characterize a sample of known HRS candidates from the literature. In Sec. 4 we show how the number of observable HRSs predicted from our model runs differ from the observed sample. In Sec. 5 we discuss the implications and limitations of our findings, and our conclusions can be found in Sec. 6.

## 2 BINARY POPULATION SYNTHESIS MODELS

We generate and evolve mock populations of massive binary systems using the population synthesis and evolution code `binary_c` ([Izzard et al. 2004, 2006, 2009](#)), based on the `binary star evolution` (BSE) code of [Hurley et al. \(2002\)](#) and the algorithms of [Tout et al. \(1997\)](#). BSE itself uses the analytical fits of [Hurley et al. \(2000\)](#) to evolutionary models of single stars from [Pols et al. \(1998\)](#). The current version of `binary_c` also includes updates from [de Mink et al. \(2013\)](#), [Schneider et al. \(2014\)](#), and [Claeys et al. \(2014\)](#) for improved models of stellar rotation, stellar lifetimes, and Roche lobe overflow mass transfer rates respectively.

We first generate a mock fiducial population, taking the same initial conditions and free physical parameters of [R19](#)’s fiducial model<sup>1</sup>, based on reasonable assumptions consistent with the current theoretical and observational understanding of the field. We briefly explain these parameters in the next subsection and refer the reader to [R19](#) for more information. Following the approach of [R19](#), we vary relevant physical parameters one-by-one to examine their impact on the number of ejected high-velocity stars. As we will see, however, the number of high-velocity ejections in the fiducial simulation is quite small. While varying individual parameters can provide valuable hints towards which parameters

are most important for high-velocity ejections, the impacts of varying individual parameters are difficult to verify robustly when comparing such small populations. We therefore instead run an ‘optimized’ simulation with all relevant free parameters optimistically tuned in directions which favour high-velocity ejections of companions. By setting parameters back to their fiducial values one-by-one, we can more confidently assess their effect on the frequency of high-velocity ejections. See Table 1 for a summary of the initial conditions and physical parameters assumed in each simulation.

### 2.1 Fiducial Model Initial Conditions and Physical Assumptions

Here we briefly define and state our assumptions for a number of initial conditions and binary evolution parameters in the fiducial model.

Each binary in our fiducial simulation is described by a zero-age main sequence (ZAMS) mass of the primary ( $M_1$ ), a ZAMS mass ratio between stars ( $q \equiv M_2/M_1$ ) and a ZAMS orbital period  $P$ . We assume that these parameters are independent from each other, although see [Moe & Di Stefano \(2017\)](#). We generate systems on a grid in this space and later statistically weigh each system, assigning each a probability according to our assumed distributions of these parameters,  $p_i \propto f(M_1)f(q)f(P)$  (see also [R19](#), Appendix B). We select primary masses logarithmically-spaced in the range  $7.5 M_\odot \leq M_1 \leq 100 M_\odot$  and statistically weigh the systems by a [Kroupa \(2001\)](#) initial mass function. ZAMS mass ratios are selected at uniform intervals in the range  $0.1 \leq q \leq 1$  assuming a probability distribution  $f(q) \propto q^\kappa$ . In the fiducial simulation we assume a flat  $q$  distribution, i.e.  $\kappa = 0$  (see e.g. [Kuiper 1935](#); [Sana et al. 2012](#); [Kobulnicky et al. 2014](#)). We draw orbital periods logarithmically-spaced in the range  $1.41 \text{ days} \leq P \leq 3.16 \times 10^5 \text{ days}$  with a probability distribution  $f(P) \propto P^\pi$ . For  $M_1 < 15 M_\odot$  we assume a flat distribution ( $\pi = 0$ ) in  $\log_{10} P$  ([Öpik 1924](#); [Kobulnicky & Fryer 2007](#)) while when  $M_1 \geq 15 M_\odot$  we assume a power law distribution in  $\log_{10} P$  with a slope  $\pi = -0.55$  ([Sana et al. 2012](#)). The lower limit on  $\log_{10} P$  is also derived from ([Sana et al. 2012](#)), while we choose an upper limit sufficiently large to include non-interacting binaries as effectively single stars ([de Mink & Belczynski 2015](#)). The orbits are always assumed to be initially circular, since close orbits are expected to circularize due to tides or mass transfer before the first CC event ([Belczyński & Bulik 1999](#); [Hurley et al. 2002](#), although see also [Eldridge 2009](#)). For all stars in the fiducial run we assume a metallicity of  $Z = 0.02$  ([Anders & Grevesse 1989](#)).

We calculate Roche lobe overflow (RLOF) mass transfer rates using the algorithm of [Claeys et al. \(2014\)](#). In this fiducial simulation, the mass transfer efficiency  $\beta_{\text{RLOF}}$  – i.e. the relative ability of an accretor with mass  $M_{\text{acc}}$  to accept mass lost by a donor at a rate  $\dot{M}_{\text{don}}$  – is set to

$$\beta_{\text{thermal}} = \min \left( \sigma \frac{\dot{M}_{\text{KH,acc}}}{\dot{M}_{\text{don}}}, 1 \right),$$

where  $\dot{M}_{\text{KH,acc}} = M_{\text{acc}}/\tau_{\text{KH}}$ ,  $\tau_{\text{KH}}$  is the Kelvin-Helmholtz timescale, and we set the parameter  $\sigma = 10$  (see [Hurley et al. 2002](#); [Claeys et al. 2014](#); [Schneider et al. 2015](#)).

The matter that is not accreted during the mass transfer leaves the system. We assume it carries with it the

<sup>1</sup> This simulation is available at [http://cdsarc.u-strasbg.fr/ftp/J/A+A/624/A66/files/A\\_fiducial.sn.dat.gz](http://cdsarc.u-strasbg.fr/ftp/J/A+A/624/A66/files/A_fiducial.sn.dat.gz).

specific angular momentum  $h$  of the accretor, i.e.  $h = \gamma_{\text{RLOF}} J_{\text{orb}} / (M_{\text{don}} + M_{\text{acc}})$ , where  $J_{\text{orb}}$  is the total angular momentum,  $M_{\text{don}}$  is the donor mass, and the loss parameter  $\gamma_{\text{RLOF}} = M_{\text{don}} / M_{\text{acc}}$  (see Soberman et al. 1997; van den Heuvel et al. 2017).

By the time the primary first fills its Roche Lobe, we assume the system enters a common envelope phase evolution (CE; Paczynski 1976) if the accretor star is sufficiently low-mass compared to the donor star ( $M_{\text{acc}} / M_{\text{don}} < q_{\text{crit}}$ ). This critical mass ratio threshold  $q_{\text{crit}}$  depends on the evolutionary stage of the donor star. We choose  $q_{\text{crit,A}} = 0.65$ ,  $q_{\text{crit,B}} = 0.4$  and  $q_{\text{crit,RSG}} = 0.25$  when the donor star is a main sequence (Case A; de Mink et al. 2007), Hertzsprung gap (Case B), and red supergiant or core helium-burning star, respectively. We note that this last  $q_{\text{crit,RSG}}$  value might be relatively low (Claeys et al. 2014), i.e. the number of CE events with giant donors might be overestimated. The conclusions of this work are insensitive to variations of this value.

Once common envelope evolution begins, we model the evolution of the system using the  $\alpha_{\text{CE}}\lambda$  formalism (see e.g. Webbink 1984; de Kool 1990; De Marco et al. 2011), wherein a fraction  $\alpha_{\text{CE}}$  of the change in orbital energy  $\Delta E_{\text{orb}}$  from the inspiraling binaries is used to eject the envelope. For the binding energy parameter  $\lambda$  we use the analytic fit to the  $\lambda_g$  values of Dewi & Tauris (2000), which do not include the thermal energy of the envelope and its potential energy due to ionization. We assume in our fiducial simulation that  $\alpha_{\text{CE}} = 1$ , i.e. all the liberated energy from the orbital inspiral is transferred to the envelope, which escapes to infinity at precisely the escape velocity from the system. Values  $\alpha_{\text{CE}} > 1$  can be used to mimic the inclusion of other sources of energy (such as accretion luminosity, recombination energy, or nuclear burning) to aid the ejection of the envelope (e.g., Ivanova 2002; De Marco et al. 2011; Ivanova et al. 2013a).

We model the reaction of a system to a CC event following Tauris & Takens (1998). We assume that supernova ejecta leave the exploding star instantaneously since the ejecta speed is much larger than the orbital velocity of the binary. The mass loss from the companion due to stripping and ablation of its envelope as a result of the ejecta impact is treated following fits to the simulations of Liu et al. (2015) with a companion mass of  $M_2 = 3.5 M_{\odot}$ .

The distribution of radio-pulsar proper motions (Shklovskii 1970; Gunn & Ostriker 1970) was the first piece of indirect evidence suggesting that asymmetries in supernova explosions could impart “natal kicks” to neutron stars at formation (Shklovskii 1970). Both asymmetric neutrino fluxes (Woosley 1987; Socrates et al. 2005) and large-scale density and velocity asymmetries in the star pre-collapse (e.g., Janka & Mueller 1994; Burrows & Hayes 1996) have been invoked to explain this natal kick, with the hydrodynamic-induced kick explanation currently more favoured over the asymmetric neutrino emission explanation (Holland-Ashford et al. 2017; Katsuda et al. 2018).

We draw natal kick magnitudes following Hobbs et al. (2005), who employ pulsar proper motions to infer that NS natal kicks follow a Maxwellian distribution with a root mean squared dispersion  $\sigma_{\text{kick}} = 265 \text{ km s}^{-1}$ . We draw natal kick directions isotropically in the frame of the collapsing star (see e.g. Wongwathanarat et al. 2013).

Since a large amount of ejecta can fall back onto the

remnant following the CC, final natal kick magnitudes must be modulated accordingly, i.e.  $v_{\text{kick}} \rightarrow v_{\text{kick}}(1 - f_{\text{b}})$ , where  $f_{\text{b}}$  is the fallback fraction. We calculate  $f_{\text{b}}$  based on the carbon-oxygen core mass of the collapsing star following the ‘rapid supernova’ algorithm of Fryer et al. (2012, hereafter F12, see their Eq. 16), which also sets the mass of the remnant. The remnant type is set by its mass; above a maximum NS mass  $M_{\text{NS,max}} = 2.5 M_{\odot}$ , the remnant is designated a black hole. The F12 algorithm generally prescribes small (large) fallback fractions when the remnant is a neutron star (black hole) and therefore large (small) kick velocities.

In the event the natal kick launches the remnant directly towards the main sequence companion, we assume that the two bodies coalesce if the remnant enters the envelope of the companion (Leonard et al. 1994), i.e. if the post-CC periastron is less than the companion star’s radius. We calculate the post-CC periastron distance following Eq. 57 of Tauris & Takens (1998), accounting for the change in momentum of the companion due to the impact of the expanding supernova shell and the stripping and ablation of the companion’s envelope. We assume a shell velocity of  $8200 \text{ km s}^{-1}$  and an escape velocity from the companion of  $800 \text{ km s}^{-1}$  (Tauris & Takens 1998). We fit to Table 1 of Wheeler et al. (1975) to determine ablation and stripping mass fractions, assuming the companion is an  $n = 3$  polytrope. In all, the impact of the supernova ejecta on the companion is a relatively small contribution to its total post-CC velocity,  $\lesssim 10 \text{ km s}^{-1}$  (Tauris & Takens 1998; Liu et al. 2015).

In total we draw 50  $M_1$ ’s  $\times$  50  $q$ ’s  $\times$  100  $P$ ’s for a total of 250,000 binary systems. As we also draw 20 natal kick magnitudes and directions as well, we end up with a mock population of  $\sim 5,000,000$  evolved binaries.

## 2.2 Optimised Model Initial Conditions and Physical Assumptions

In addition to the fiducial model we also run a simulation with initial conditions and physics tuned to enhance the occurrence of high velocity ejections of companions from disrupted binaries. We discuss in Sec. 5.1 whether these tunings are consistent with contemporary observations and theory. If the size of the currently-known sample of HRS candidates cannot be matched by even this ad-hoc scenario, the BSS mechanism can be conclusively ruled out as a significant provenance for Milky Way HRSS. When a binary system is disrupted, the ejection velocity of the companion star is similar to its pre-CC orbital velocity (Blaauw 1961; Eldridge et al. 2011; R19). The philosophy behind many of our changes to the initial conditions and physical parameters is therefore a) to increase the companion’s pre-CC velocity as much as possible, and b) to increase the rate of binary disruption. Increasing the companion’s orbital velocity implies producing harder binaries, which decreases the ease with which binaries are ionized. Indeed, tighter binaries may preferentially merge or remain bound and we therefore attempt to enhance the occurrence of physical configurations that specifically avoid those fates.

Stable RLOF mass transfer can lead to orbital widening as the system tends towards equal star mass. We suppress this by setting  $\beta_{\text{RLOF}} = 0$ . We also set  $\gamma_{\text{RLOF}} = 1$  to increase the amount of angular momentum sapped from the system by escaping material compared to our fiducial setup.



Since common envelope evolution leads to orbital tightening, we want to encourage the occurrence of this phase but simultaneously avoid binary mergers. We achieve this by choosing  $\alpha_{\text{CE}} = 10$  – the maximum of the  $\alpha_{\text{CE}}$  range suggested by Hurley et al. (2002) – and also choosing  $q_{\text{crit}} = 1$  regardless of donor type. A CE efficiency greater than 1 might be achieved by tapping extra energy sources, e.g. in the thermal motions and ionization state of the envelope (De Marco et al. 2011; Ivanova et al. 2013a,b, see also Sec. 5.1.2).

Another physical ingredient that can in principle lead to tighter binaries is metallicity. At fixed stellar mass, stellar radii are smaller in metal-poor stars (see e.g. Burrows et al. 1993; Pols et al. 1998). Binary systems composed of smaller stars enter the mass transfer stage later and experience less orbital widening, and are also able to orbit at smaller separations without merging both of which lead to faster orbital velocities (R19). In the optimized simulation we set the total stellar metallicity to  $Z = 0.0063$ , one-half dex lower than our fiducial value of  $Z = 0.02$ .

Finally, to increase the frequency of binary disruption, we boost the Maxwellian kick distribution dispersion to  $\sigma_{\text{kick}} = 1000 \text{ km s}^{-1}$  and set all fallback fractions to zero. We also set both the ZAMS mass ratio and initial log-period distribution slopes to  $\pi = \kappa = -1$  to enhance the frequency of configurations where the companion has a large orbital velocity at ZAMS.

### 2.3 Other Model Variations

Our predictions depend on initial conditions for the binary systems and parametrized assumptions for binary evolution physics. In addition to the fiducial and optimized simulations, we run simulations where we vary these free parameters one-by-one<sup>2</sup>. We set one parameter to its fiducial value while keeping all others set to their optimized value to explore the impact each parameter has on the rate of high-velocity star ejections.

To determine whether a common envelope efficiency  $1 < \alpha_{\text{CE}} < 10$  is more effective than  $\alpha_{\text{CE}} = 10$  at encouraging orbital tightening while avoiding mergers, we additionally perform a run with all parameters set to their optimized value except  $\alpha_{\text{CE}}$  is set to 5.

To explore the possibility that the low-mass cores of less massive NSs experience smaller natal kicks as suggested by some authors (e.g., Katz 1975; Arzoumanian et al. 2002; Pfahl et al. 2002; Podsiadlowski et al. 2004; Verbunt et al. 2017; Vigna-Gómez et al. 2018), we additionally perform a run with all parameters set to their optimized value except the natal kick is drawn from a double-peaked Maxwellian distribution similar to Vigna-Gómez et al. (2018) (see also R19). Following Pfahl et al. (2002) and Podsiadlowski et al. (2004), we draw from a kick distribution with  $\sigma_{\text{kick,low}} = 30 \text{ km s}^{-1}$  for remnants less massive than  $1.35 M_{\odot}$  (Schwab et al. 2010; Knigge et al. 2011) while the kick distribution for more massive remnants remains at  $\sigma_{\text{kick,high}} = 265 \text{ km s}^{-1}$ .

Table 1 summarizes the initial conditions and parameters assumed in each simulation.

### 2.4 Comparisons to Data

Each simulation contains a number  $N_f$  of systems which eject a companion at a high velocity, here defined as  $v_{\text{ej}} \geq 400 \text{ km s}^{-1}$ . Properly accounting for the probabilities of each system and the finite stellar lifetimes of the ejected companions, we convert this to a number  $N_{f,\text{now}}$  of stars in the Galaxy today with the same cut in ejection velocity. We estimate the number of systems – consisting of either isolated stars or binaries – that are formed per unit time in the Milky Way as  $\langle SFR \rangle / \langle M \rangle$ : we assume a constant star formation rate of  $\langle SFR \rangle = 3.5 M_{\odot} \text{ yr}^{-1}$  (see e.g. Dominik et al. 2012) and the probability-weighted mean mass of a system is calculated as

$$\langle M \rangle = \langle M_1(1+q) \rangle = \langle M_1 \rangle + \langle qM_1 \rangle \quad (1)$$

$$\langle M \rangle = \frac{\int_{0.01}^{100} M_1 f(M_1) dM_1}{\int_{0.01}^{100} f(M_1) dM_1} + \frac{\int_2^{100} M_1 f(M_1) dM_1}{\int_{0.01}^{100} f(M_1) dM_1} \frac{\int_{0.1}^1 q f(q) dq}{\int_{0.1}^1 f(q) dq}, \quad (2)$$

where  $f(M_1)$  is a Kroupa (2001) initial mass function,  $f(q) \propto q^{\kappa}$  is the distribution of ZAMS mass ratios, and where we assume a binary fraction of 0 for  $M_1 < 2 M_{\odot}$  and 1 for  $M_1 \geq 2 M_{\odot}$ . Eq. 2 gives  $\langle M \rangle = 0.64 M_{\odot}$  for  $\kappa = -1$  and  $0.68 M_{\odot}$  for  $\kappa = 0$ . Therefore, the birth rate of systems is  $\langle SFR \rangle / \langle M \rangle \approx 5.1 - 5.5 \text{ yr}^{-1}$ . A fraction  $F_f$  of those systems eject fast stars. We calculate this by summing over the statistical weights  $p_i$  of each sampled system that produces a fast star in our simulation given its initial configuration:  $p_i \propto f(M_1)f(q)f(P)$ :

$$F_f = \sum_i^{N_f} p_i. \quad (3)$$

These fast-ejected companions survive for a probability-weighted average time  $\langle t_{\text{flight}} \rangle$ ,

$$\langle t_{\text{flight}} \rangle = \frac{\sum_i^{N_{\text{fast}}} \Delta t_{\text{left},i} \cdot p_i}{\sum_i^{N_{\text{fast}}} p_i}, \quad (4)$$

where  $\Delta t_{\text{left},i}$  is the remaining main sequence lifetime of the  $i$ -th fast-ejected companion. Putting this all together, the number  $N_{f,\text{now}}$  of BSS-ejected fast stars in the Milky Way at any given time in the whole sky is therefore

$$N_{f,\text{now}} = F_f \frac{\langle SFR \rangle}{\langle M \rangle} \langle t_{\text{flight}} \rangle. \quad (5)$$

To roughly estimate a number  $N_{f,\text{obs}}$  of fast companions currently *observable* in the whole sky, we cap  $\Delta t_{\text{left}}$  at 100 Myr under the assumption that fast stars with  $\Delta t_{\text{left}} > 100 \text{ Myr}$  will be too far (and therefore too faint) to be detected at their current distances. This cap at 100 Myr is chosen to match more or less the maximum travel time seen in the current sample of observed hyper-runaway star candidates (see Sec. 3).

An alternative method to estimate  $N_{f,\text{now}}$  would be to assume a CC supernova rate of  $\sim 1.9$  per century in the Milky Way (Diehl et al. 2006). Assuming all and only  $M > 8 M_{\odot}$  stars undergo CC supernovae, we can re-express  $F_f$  as a fraction only of  $M_1 > 8 M_{\odot}$  systems. Doing this and swapping  $\langle SFR \rangle / \langle M \rangle$  for the CC supernova rate in Eq. 5 yields very similar estimates for  $N_{f,\text{now}}$ .

<sup>2</sup> Upon publication, all simulations will be publicly available at the DOI: [10.5281/zenodo.3860055](https://doi.org/10.5281/zenodo.3860055)

**Table 1.** Summary of the input parameters to our binary synthesis models - the zero age main sequence (ZAMS) mass ratio distribution slope ( $\kappa$ ), the ZAMS log-period distribution slope ( $\pi$ ), the Roche lobe overflow (RLOF) mass transfer efficiency ( $\beta_{\text{RLOF}}$ ), the RLOF angular momentum loss parameter ( $\gamma_{\text{RLOF}}$ ), the critical mass ratio for common envelope evolution ( $q_{\text{crit}}$ ), the common envelope efficiency ( $\alpha_{\text{CE}}$ ), the RMS dispersion of the natal kick Maxwellian distribution ( $\sigma_{\text{kick}}$ ), the post-kick fallback fraction ( $f_{\text{b}}$ ) and the total stellar metallicity ( $Z$ ). See Sec. 2 for details.

Model	$\kappa$	$\pi$	$\beta_{\text{RLOF}}$	$\gamma_{\text{RLOF}}$	$q_{\text{crit}}$	$\alpha_{\text{CE}}$	$\sigma_{\text{kick}}$ [km s $^{-1}$ ]	$f_{\text{b}}$	$Z$
Fiducial	0	0 for $M_1 < 15 M_{\odot}$ -0.55 for $M_1 \geq 15 M_{\odot}$	$\beta_{\text{thermal}}$	$M_{\text{don}}/M_{\text{acc}}$	0.65 for case A 0.4 for case B 0.25 for giant donors	1	265	F12	0.02
Optimized	-1	-1	0	1	1	10	1000	0	0.0063
Opt. BUT $\kappa$ fiducial	0	-1	0	1	1	10	1000	0	0.0063
Opt. BUT $\pi$ fiducial	-1	0 for $M_1 < 15 M_{\odot}$ -0.55 for $M_1 \geq 15 M_{\odot}$	0	1	1	10	1000	0	0.0063
Opt. BUT $\beta_{\text{RLOF}}$ fiducial	-1	-1	$\beta_{\text{thermal}}$	1	1	10	1000	0	0.0063
Opt. BUT $\gamma_{\text{RLOF}}$ fiducial	-1	-1	0	$M_{\text{don}}/M_{\text{acc}}$	1	10	1000	0	0.0063
Opt. BUT $q_{\text{crit}}$ fiducial	-1	-1	0	1	0.65 for case A 0.4 for case B 0.25 for giant donors	10	1000	0	0.0063
Opt. BUT $\alpha_{\text{CE}}$ fiducial	-1	-1	0	1	1	1	1000	0	0.0063
Opt. BUT $\alpha_{\text{CE}} = 5$	-1	-1	0	1	1	5	1000	0	0.0063
Opt. BUT $\sigma_{\text{kick}}$ fiducial	-1	-1	0	1	1	10	265	0	0.0063
Opt. BUT $f_{\text{b}}$ fiducial	-1	-1	0	1	1	10	1000	F12	0.0063
Opt. BUT $Z$ fiducial	-1	-1	0	1	1	10	1000	0	0.02
Opt. BUT bimodal kick	-1	-1	0	1	1	10	30 for $M_{\text{remnant}} \leq 1.35 M_{\odot}$ 265 for $M_{\text{remnant}} > 1.35 M_{\odot}$	0	0.0063

### 3 SAMPLE OF GALACTIC HYPER-RUNAWAY STAR CANDIDATES

Our sample of Milky Way hyper-runaway candidates is derived from the Open Fast Stars Catalog<sup>3</sup> (OFSC; see Boubert et al. 2018), constructed using the AstroCats framework (Guillochon et al. 2017). The OFSC is a curated catalog of  $\sim 500$  hyper-velocity star candidates of all types, combining *Gaia* astrometry and photometry with supplementary properties such as stellar types and radial velocities from the literature. Spectra for each object are provided when available, from e.g. SDSS (Abolfathi et al. 2018) or LAMOST (Luo et al. 2016).

We extract full 6D observations (position, proper motions, spectroscopic distance and radial velocity) from the OFSC for the 68 high-velocity star candidates of spectral type A or B. For spectral types we refer only to the most recently published type for each star. We remove stars identified via colour-colour or  $T_{\text{eff}}$  vs.  $\log[g]$  selection cuts, it can be difficult to distinguish between early-type main sequence stars and lower-mass blue horizontal branch (BHB) stars since they populate similar regions of the Hertzsprung-Russell diagram (see e.g., Brown et al. 2006; Heber et al. 2008a; Brown et al. 2009). Projected rotational velocities and helium abundances derived via high-resolution spectra can break this degeneracy (see Heber et al. 2008a; Irrgang et al. 2018; Hattori et al. 2019). In cases where this ambiguity exists, we assume the star to be main sequence. *Gaia* proper motions are used for every star, though for HVS1, HVS10, HVS12 and HVS13 (Brown et al. 2009) we also explore using the *Hubble* Space Telescope (HST) proper motion measurements of Brown et al. (2015), as they are more precise than the *Gaia* measurements even when  $\pm 0.5 \text{ mas yr}^{-1}$  is added in quadrature to the uncertainties as suggested by Brown et al. (2018). We remove HVS11 and HVS14 (Brown et al. 2009) as well as HVS23 (Brown et al. 2014), for whom no proper motion measurements exist in the literature. When multiple distance or radial velocity measurements are provided, we take the value most recently published as of writing. For the 9 stars without explicit radial velocity uncertainties in Brown et al. (2009, 2012), we assume the reported  $\pm 11 \text{ km s}^{-1}$  average uncertainty. We do the same for LMST-HVS12 and LMST-HVS19, assuming  $\pm 13 \text{ km s}^{-1}$  as the reported average uncertainty in Zhong et al. (2014). We keep sky positions for each star fixed and perform Monte Carlo (MC) resamplings over the remaining astrometric parameters, assuming Gaussian distributions and accounting for correlation between the proper motion components.

We integrate 1000 MC realizations for each of our A- and B-type hyper-runaway candidates backwards in time up to a maximum of 1 Gyr at a fixed 0.1 Myr timestep in the *MWPotential2014* potential outlined in Bovy (2015), a three-component potential model consisting of a spherical power law bulge potential, Miyamoto-Nagai disc (Miyamoto & Nagai 1975) and spherical NFW halo (Navarro et al. 1996). *MWPotential2014* assumes a circular velocity at the Solar position of  $220 \text{ km s}^{-1}$  and a distance between the Sun and the Galactic Centre of 8 kpc. We assume local standard of rest UVW velocities of (11.1, 12.24, 7.25)  $\text{km s}^{-1}$  (Schönrich

et al. 2010) and a height of the Sun above the stellar disc of 25 pc (Bland-Hawthorn & Gerhard 2016). We do not consider uncertainties in the Solar position or velocity, though we verify that these do not meaningfully affect our results. For the orbital traceback of each MC realization we determine the location of the last disc crossing, i.e. the  $(x_{\text{GC}}, y_{\text{GC}})$  position when  $z_{\text{GC}} = 0$  in a Galactocentric Cartesian frame. For each realization we also track  $t_f$  – the flight time from the disc crossing location to the observed position – and the ejection velocity  $v_{\text{ej}}$  in both the Galactocentric Cartesian frame and in the frame of the rotating disc. Ejection velocities in the corotating frame are computed using the rotational velocity curve associated to the *MWPotential2014* potential. For MC realizations dynamically bound to the Milky Way, we record the location, velocity and flight time of each and every disc crossing up until the estimated main sequence lifetime of the star.

For each star in our sample we compute the probability  $P_{\text{disc}}$  of being ejected from the Milky Way disc by taking the fraction of MC realizations which cross the disc at a Galactocentric distance  $1 \text{ kpc} \leq r_{\text{GC}} \leq 25 \text{ kpc}$ , imposing the cut at 1 kpc to remove stars ejected from the Galactic Centre and taking 25 kpc as the edge of the stellar disc (Xu et al. 2015). We also compute the probability  $P_{v>400\text{km/s}}$  of a ‘fast’ ejection by taking the fraction of MC realizations which are ejected in the corotating frame at  $\geq 400 \text{ km s}^{-1}$ . This cut at  $400 \text{ km s}^{-1}$  is commonly cited as a limit for classical ejection mechanisms (see Irrgang et al. 2018, 2019, and references therein). This is a somewhat arbitrary velocity cut but our conclusions on the nature of the observed HRSs do not depend on the choice of the velocity threshold as long as it remains above a few hundreds  $\text{km s}^{-1}$ .

We select our early-type HRS candidates as those stars in our sample for which  $P_{\text{disc}} > 70\%$  and  $P_{v>400\text{km/s}} > 70\%$ . We additionally require that the Galactic Centre does not lie within the  $1\sigma$  contour of the disc crossing location distribution. Our sample with these cuts applied results in 14 stars. The names, astrometry and spectral types of these stars can be seen in Table 2. We show as well the probability  $P_{\text{ub}}$  of each HRS candidate to be unbound from the Galaxy, taken as the fraction of MC realizations whose total Galactocentric velocities exceed the *MWPotential2014* escape velocity at their position. We also include in our sample as a special exception the oft-cited HRS candidate HD 271791, whose high space velocity, likely disc origin, and  $\alpha$ -element enhancement are taken as evidence for a BSS ejection (Przybilla et al. 2008b). Note, however, that the natal kick velocity required in this case must be very large (Gvaramadze 2009). With an ejection velocity in the corotating frame of  $390^{+70}_{-30} \text{ km s}^{-1}$ , it just barely fails our  $P_{v>400\text{km/s}} > 70\%$  cut.

<sup>3</sup> <https://faststars.space/>

**Table 2.** Observed properties of HRS candidates with a probability  $>70\%$  of being ejected from the Milky Way disc at a velocity  $>400\text{ km s}^{-1}$  in the corotating frame.  $P_{\text{ub}}$  gives the probability of each star being unbound from the Milky Way (see text).  $v_{\text{GC}}$  is the star's current total velocity in a Galactic Cartesian reference frame. Stars above the solid separating line only cross the Galactic disk within the nominal stellar lifetime of a star of their mass.

Name	Spec. Type	(RA, Dec.) ( $^{\circ}$ )	$\mu_{\alpha*}$ (mas/yr)	$\mu_{\delta}$ (mas/yr)	d (kpc)	$v_{\text{radial}}$ (km s $^{-1}$ )	$v_{\text{GC}}$ (km s $^{-1}$ )	$P_{\text{ub}}$	Ref.
B485	A0	(152.578, 30.341)	$-0.866 \pm 0.164$	$-0.108 \pm 0.159$	$33.0^{+4.0}_{-3.0}$	$422.7 \pm 1.8$	$439^{+16}_{-13}$	1.0	1, 2
B733	B	(222.482, 31.064)	$-1.227 \pm 0.080$	$-4.521 \pm 0.125$	$12.0 \pm 1.0$	$351.4^{+2.2}_{-2.0}$	$460^{+5}_{-4}$	0.3	2, 3
HVS5	B	(139.498, 67.377)	$-0.023 \pm 0.195$	$-1.179 \pm 0.297$	$37.0 \pm 4.0$	$541.5 \pm 5.9$	$643^{+6}_{-6}$	1.0	2, 4
HVS8	B	(145.558, 20.056)	$-0.972 \pm 0.403$	$+0.117 \pm 0.407$	$36.0 \pm 3.0$	$498.9^{+3.3}_{-3.1}$	$483^{+54}_{-32}$	1.0	2, 3
HVS17	B	(250.485, 47.396)	$-1.034 \pm 0.223$	$-1.065 \pm 0.364$	$35.0 \pm 3.0$	$255.5 \pm 3.0$	$448^{+19}_{-12}$	1.0	2, 5
LAMOST-HVS1	B1	(138.027, 9.273)	$-3.537 \pm 0.213$	$-0.62 \pm 0.180$	$13.4^{+1.7}_{-1.5}$	$611.7 \pm 4.6$	$553^{+13}_{-13}$	1.0	6, 7, 8
LAMOST-HVS2	B2	(245.087, 37.794)	$-2.563 \pm 0.086$	$-0.924 \pm 0.111$	$22.2 \pm 4.6$	$341.1 \pm 7.8$	$506^{+16}_{-12}$	1.0	7
LAMOST-HVS4	B6	(344.657, 40.001)	$+0.343 \pm 0.110$	$-0.288 \pm 0.120$	$27.9 \pm 1.5$	$359.0 \pm 7.0$	$574^{+7}_{-7}$	1.0	9
SDSSJ013655.91+242546.0	A	(24.233, 24.429)	$-1.985 \pm 0.169$	$-6.688 \pm 0.116$	$9.9 \pm 2.0$	$300.7 \pm 1.5$	$521^{+30}_{-28}$	0.97	10, 11
SDSSJ115245.91+021116.2	B	(178.191, -2.188)	$-0.123 \pm 0.555$	$+0.171 \pm 0.249$	$30.4 \pm 5.0$	$424.0 \pm 11.0$	$384^{+29}_{-23}$	0.42	3, 12
HD 271791	B2/B3	(90.616, -66.791)	$-0.619 \pm 0.083$	$+4.731 \pm 0.088$	$20.4 \pm 3.9$	$441.0 \pm 1.0$	$524^{+77}_{-78}$	0.88	13
PG1610+062	B6	(243.222, 6.094)	$-0.616 \pm 0.109$	$+0.176 \pm 0.060$	$17.3^{+2.9}_{-2.5}$	$157.4 \pm 7.7$	$306^{+8}_{-8}$	0.00	14
LMST-HVS9	A6	(206.590, 30.263)	$-15.795 \pm 0.115$	$-62.689 \pm 0.067$	$1.8 \pm 0.2$	$-186.5 \pm 0.7$	$387^{+63}_{-62}$	0.02	15, 16
LMST-HVS19	A0	(340.533, 7.469)	$+63.831 \pm 0.129$	$-39.117 \pm 0.086$	$1.2 \pm 0.1$	$-436.0 \pm 13.0$	$399^{+24}_{-23}$	0.00	15, 16
LMST-HVS24	A7	(320.118, -1.557)	$+49.096 \pm 0.145$	$-48.834 \pm 0.107$	$1.2 \pm 0.2$	$-301.3 \pm 56.4$	$331^{+50}_{-47}$	0.0003	15, 16

**References.** (1) Brown et al. (2015), (2) Kreuzer et al. (2020), (3) Brown et al. (2007), (4) Brown et al. (2006), (5) Brown et al. (2012), (6) Zheng et al. (2014), (7) Huang et al. (2017), (8) Hattori et al. (2019), (9) Li et al. (2018), (10) Tillich et al. (2009), (11) Alam et al. (2015), (12) Brown et al. (2009), (13) Heber et al. (2008b), (14) Irrgang et al. (2019), (15) Zhong et al. (2014), (16) Luo et al. (2016)

**Table 3.** Disc-crossing properties of 15 HRS candidates with a probability  $>70\%$  of being ejected from the Galactic disc at a velocity  $>400\text{ km s}^{-1}$  in the corotating frame. Uncertainties represent  $1\sigma$  error intervals. Stars below the solid line cross the Galactic disc more than once within the estimated lifetime of a star with their mass. For such stars we only show the disc crossing properties for the most recent crossing.  $v_{\text{ej,corotating}}$  denotes ejection velocities in the corotating frame of the Milky Way disc.  $P_{\text{disc}}$  denotes the probability that the star is ejected from a Galactocentric distance  $1\text{ kpc} \leq r_{\text{GC}} \leq 25\text{ kpc}$ .  $P_{v>400\text{km/s}}$  denotes the probability of that the star is ejected at  $v_{\text{ej,corotating}} \geq 400\text{ km s}^{-1}$ .

Name	<i>Gaia</i> DR2 ID	$r_{\text{GC}}$ (kpc)	$v_{\text{ej}}$ (km s $^{-1}$ )	$v_{\text{ej,corotating}}$ (km s $^{-1}$ )	$t_{\text{flight}}$ (Myr)	$P_{\text{disc}}$	$P_{v>400\text{km/s}}$
B485	742363828436051456	$13.4^{+3.9}_{-2.2}$	$520^{+4}_{-4}$	$410^{+12}_{-6}$	$86^{+8}_{-12}$	0.99	0.99
B733	1283080527168129536	$10.8^{+0.6}_{-0.5}$	$479^{+5}_{-5}$	$459^{+8}_{-8}$	$27^{+2}_{-2}$	1.00	1.00
HVS17	1407293627068696192	$14.2^{+3.7}_{-4.3}$	$523^{+15}_{-8}$	$415^{+25}_{-16}$	$64^{+7}_{-5}$	1.00	0.83
HVS5	1069326945513133952	$8.9^{+2.4}_{-3.2}$	$733^{+30}_{-15}$	$674^{+88}_{-67}$	$54^{+6}_{-5}$	1.00	1.00
HVS8	633599760258827776	$16.1^{+9.4}_{-5.3}$	$557^{+16}_{-10}$	$443^{+39}_{-22}$	$83^{+12}_{-11}$	0.83	1.00
LAMOST-HVS1	590511484409775360	$3.2^{+2.6}_{-1.0}$	$684^{+20}_{-30}$	$570^{+19}_{-22}$	$35^{+6}_{-6}$	1.00	1.00
LAMOST-HVS2	1330715287893559936	$6.8^{+2.3}_{-1.0}$	$600^{+10}_{-11}$	$539^{+25}_{-41}$	$34^{+4}_{-5}$	1.00	1.00
LAMOST-HVS4	1928660566125735680	$8.6^{+0.9}_{-0.6}$	$658^{+9}_{-9}$	$464^{+14}_{-9}$	$50^{+4}_{-4}$	1.00	1.00
SDSSJ013655.91+242546.0	291821209329550464	$13.6^{+1.7}_{-1.7}$	$532^{+30}_{-27}$	$461^{+43}_{-48}$	$13^{+1}_{-1}$	1.00	0.91
SDSSJ115245.91-021116.2	3602104614919092736	$15.7^{+6.2}_{-3.0}$	$444^{+19}_{-16}$	$478^{+22}_{-25}$	$61^{+13}_{-9}$	0.94	1.00
HD 271791	5284151216932205312	$12.7^{+6.4}_{-4.1}$	$545^{+60}_{-41}$	$390^{+70}_{-26}$	$35^{+6}_{-6}$	0.97	0.43
PG1610+062	4450123955938796160	$6.4^{+1.3}_{-0.9}$	$403^{+10}_{-10}$	$519^{+27}_{-39}$	$44^{+9}_{-9}$	1.00	0.99
LMST_HVS9	1455666400613902976	$10.1^{+3.9}_{-3.4}$	$317^{+12}_{-3}$	$473^{+34}_{-19}$	$422^{+291}_{-168}$	1.00	1.00
LMST_HVS19	2715682777307050240	$9.6^{+3.0}_{-2.2}$	$376^{+50}_{-55}$	$550^{+73}_{-73}$	$34^{+14}_{-11}$	1.00	0.99
LMST_HVS24	2686125426556270592	$6.6^{+0.2}_{-0.3}$	$355^{+51}_{-49}$	$533^{+63}_{-61}$	$4^{+1}_{-1}$	1.00	0.99



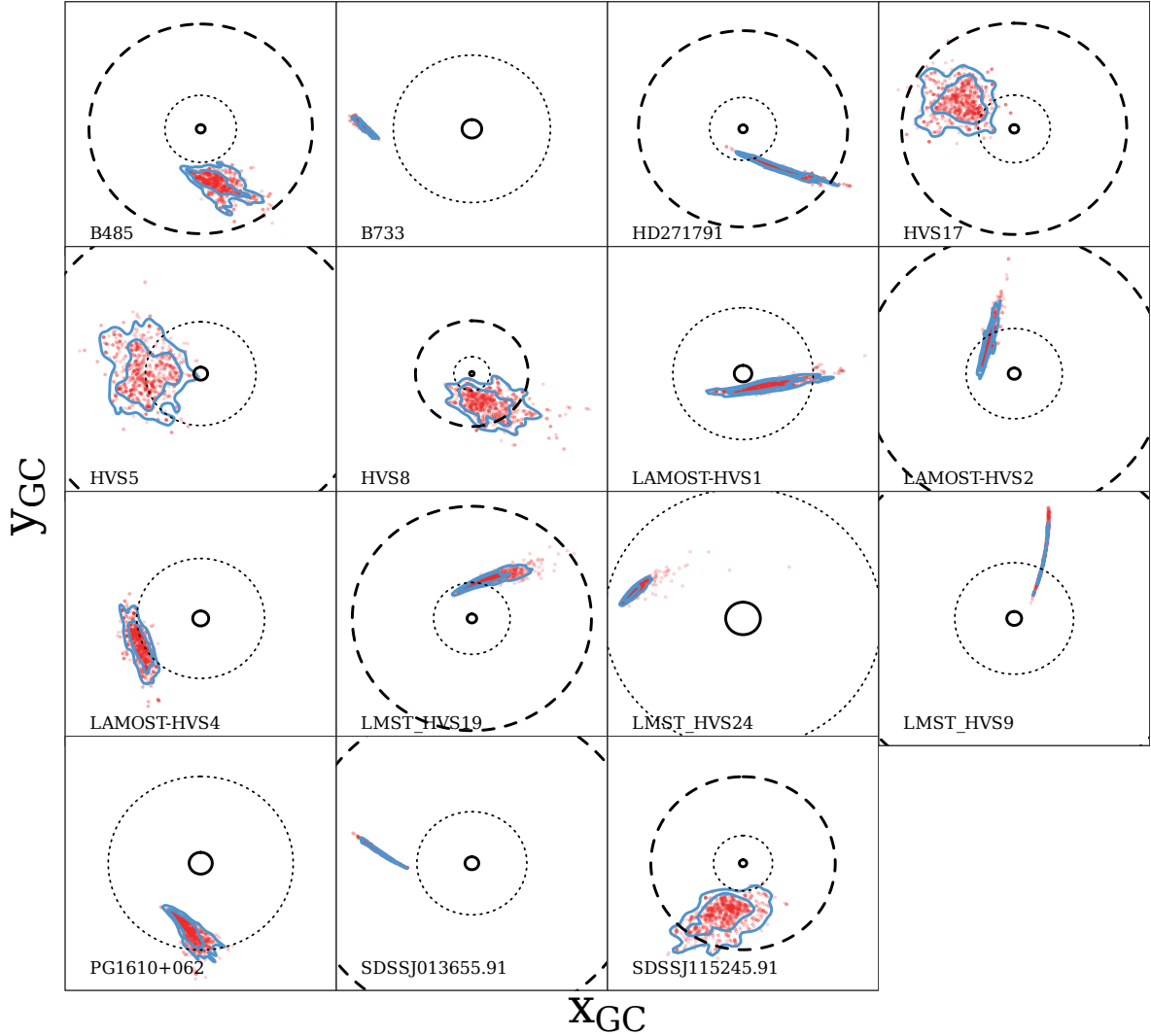


**Figure 1.** Red points show most recent disc-crossing locations for 1000 Monte Carlo realizations of our HRS candidates. Blue contours show  $1\sigma$  and  $2\sigma$  confidence intervals of the disc-crossing location distributions. The solid inner, dotted middle and dashed outer rings have radii of 1 kpc, 8 kpc and 25 kpc respectively (not shown in all panels).

The Galactocentric Cartesian ( $y_{GC}, y_{GC}$ ) locations of the most recent disc crossing for each MC realization of each star can be seen in Fig. 1. They range from stars ejected from a tightly-constrained region of the disc (e.g. B733) to stars with wide spreads of possible birthplaces (e.g. SDSS J115245.91-021116.2). In Fig. 2 we show the distributions of corotating ejection velocities for each hyper-runaway candidate. 12 of our 15 stars only cross the Galactic disc once within their estimated main sequence lifetime. The possible ejection locations, velocities and flight times for the first crossing for each star are summarized in Table 3. With the exception of LMST\_HVS9 (Zhong et al. 2014; Luo et al. 2016) which is currently on an inbound orbit, every star in our sample has crossed the Milky Way disc within the last  $\sim 100$  Myr.

This sample of HRS candidates is neither volume- nor magnitude-limited. Since our sample is drawn from a variety of surveys and targeted searches with different sky coverage and completeness limits, we do not attempt to correct for

these biases to determine a robust, corrected estimate for the number of HRS candidates in the Milky Way. Rather, this sample serves as a useful low-end estimate against which we compare the number of HRSs predicted by our binary population synthesis simulations.

#### 4 RESULTS

We select from our simulations the main sequence companions ejected from disrupted binary systems, i.e. from systems which did not undergo a merger and did not stay bound after the CC of the primary. We further remove those systems which experience a collision between the remnant and the companion star post-CC (see Sec. 2.1). We show in Fig. 3 how these ejected companions populate the  $v_{ej}$ - $M$  space for both the fiducial (Sec. 2.1) and optimized (Sec. 2.2) simulations, with the other models described in Sec. 2.3 not shown for brevity. We include for reference the ejection velocities

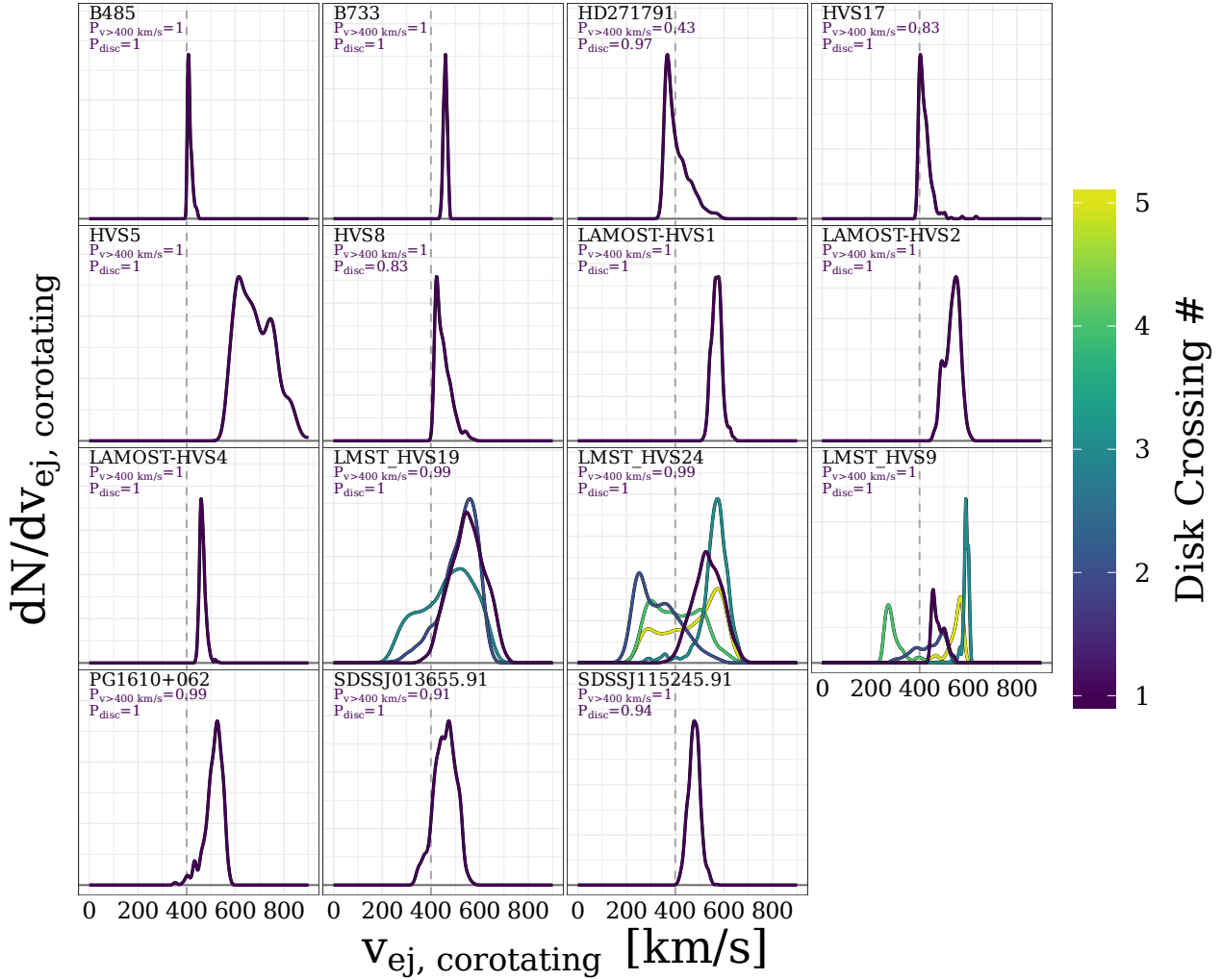


**Figure 2.** Distribution of ejection velocities in the corotating frame from the Milky Way disc for 1000 Monte Carlo (MC) realizations of 15 HRS candidates. Different colours denote separate disc crossings, starting with the most recent. Shown for each star are  $P_{v>400\text{km/s}}$ , the fraction of MC realizations where the star is ejected from the Milky Way disc during the most recent disc crossing at  $>400\text{ km s}^{-1}$  in the corotation frame, and  $P_{\text{disc}}$ , the fraction of MC realizations where the star is ejected during the most recent disc crossing from a Galactocentric distance  $1\text{ kpc} \leq r_{\text{GC}} \leq 25\text{ kpc}$ . See Table 3 for more disc-crossing properties for each star.

(in the corotating disc frame) and stellar masses of the 15 stars in our sample of observed HRS candidates. Notice in the fiducial model (left panel) that the bulk of main sequence companions are ejected at  $\sim 10\text{ km s}^{-1}$  regardless of mass, as reported in R19. There is in fact only a single main sequence companion in the fiducial model that is ejected at  $\geq 400\text{ km s}^{-1}$ . By Eq. 5, this model predicts  $N_{\text{f,now}} = 8$  HRSs currently in the Milky Way and one BSS-ejected HRS currently observable, clearly at odds with the current known population of HRS candidates without even accounting for magnitude limits and sky coverage.

For the optimized model shown in the right panel of Fig. 3, notice that although the main peak of the  $v_{\text{ej}}$  distribution is still at  $\sim 10\text{ km s}^{-1}$ , there is a second peak near  $v_{\text{ej}} \approx 100\text{ km s}^{-1}$  with a high-velocity tail extending past our cut at  $v_{\text{ej}} = 400\text{ km s}^{-1}$ . The probability  $F_{\text{f}}$  described by Eq. 3 of ejecting a fast companion is  $1.77 \times 10^{-5}$  in the optimized simulation,  $\sim 1.4 \times 10^4$  times more likely than in the fiducial simulation. This optimized simulation predicts

$N_{\text{f,now}} \simeq 1.2 \times 10^4$  HRSs in the Milky Way, 5590 ejected less than 100 Myr ago – many more than the 15 HRS candidates in our observed sample. These typically have masses greater than  $\sim 2 M_{\odot}$ , with a broad peak around  $\sim 10 M_{\odot}$  that extends to the highest masses we probe. At the lower end, the masses of HRSs might be in part limited by our choice of minimum ZAMS mass ratio ( $q = M_2/M_1 \geq 0.1$ , see also Sec. 5.3). We point out that the former companions of these stars are even more massive, with a pre-CC mass distribution peaking at  $\sim 30 M_{\odot}$ . The typical progenitor binaries of fast stars are therefore quite massive overall. We come back to this later in this section.

The results for the fiducial and optimized simulations as well as all other simulations described in Sec. 2.3 are summarized in Table 4. We show the probability  $F_{\text{f}}$  of systems in the simulation to eject a companion at  $v_{\text{ej}} \geq 400\text{ km s}^{-1}$  (see Eq. 3) along with the predicted number  $N_{\text{f,now}}$  of  $v_{\text{ej}} \geq 400\text{ km s}^{-1}$  stars in the Milky Way today and the number  $N_{\text{f,obs}}$  with flight times less than 100 Myr (see Eq. 5).

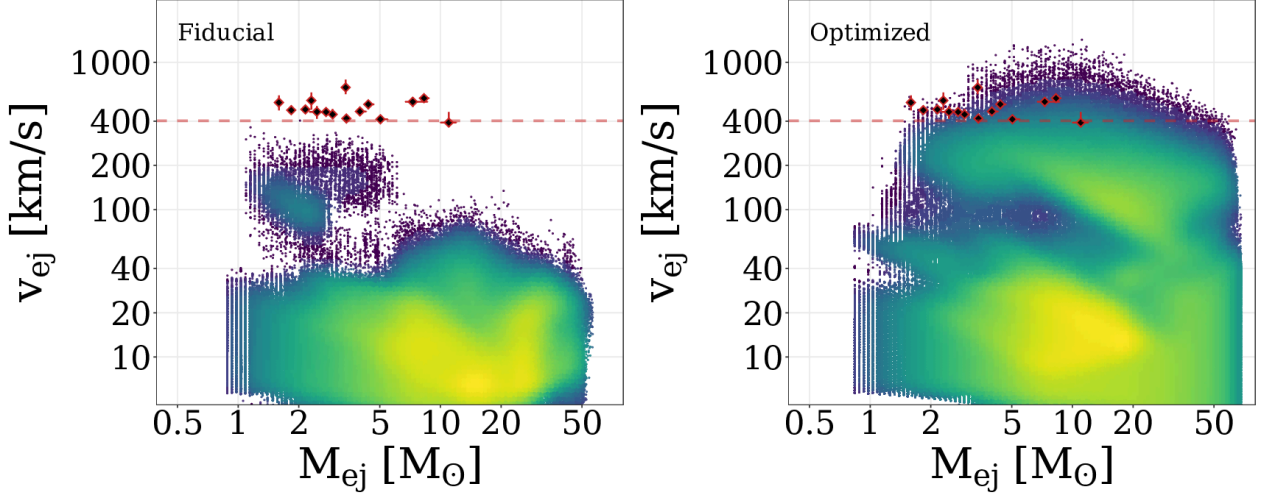


**Figure 3.** Ejection velocity  $v_{\text{ej}}$  of ejected main sequence companions following a core-collapse (CC) event as a function of their mass  $M_{\text{ej}}$  in our fiducial (left) and optimized (right) simulations. Colour is proportional to logarithmic number density. Note that features at  $M_{\text{ej}} \sim 1 M_{\odot}$  are artifacts of the `binary_c` grid. Horizontal dashed line corresponds to  $v_{\text{ej}} = 400 \text{ km s}^{-1}$ . Black-and-red points show ejection velocities (in the disc corotating frame) and masses of 15 HRS candidates. Vertical error bars are  $1\sigma$  range in ejection velocities from 1000 Monte Carlo realizations. Horizontal error bars are mass uncertainties.

**Table 4.** Summary of the frequency of fast ejections seen in the simulations described in Sec. 2 and summarized in Table. 1. We include the per-system probability  $F_{\text{f}}$  of a  $\geq 400 \text{ km s}^{-1}$  ejection, the number  $N_{\text{f,now}}$  of  $v_{\text{ej}} \geq 400 \text{ km s}^{-1}$  hyper-runaway stars these simulations predict to be in the Milky Way today (see Eq. 5), the predicted number  $N_{\text{f,obs}}$  of stars with a flight time less than 100 Myr, and the predicted fraction  $f_{15}^{\text{RW}}$  of all  $M > 15 M_{\odot}$  stars which are  $v_{\text{ej}} > 30 \text{ km s}^{-1}$  runaways (see text).

Model	$F_{\text{f}}$	$N_{\text{f,now}}$	$N_{\text{f,obs}}$	$f_{15}^{\text{RW}}$
Fiducial	$1.26 \times 10^{-9}$	8	1	0.54%
Optimized	$1.77 \times 10^{-5}$	11767	5590	1.63%
Opt. BUT $\gamma$ fiducial	$1.79 \times 10^{-5}$	12492	5728	1.60%
Opt. BUT $\beta$ fiducial	$1.78 \times 10^{-5}$	13384	5671	1.46%
Opt. BUT $\pi$ fiducial	$2.01 \times 10^{-5}$	14575	6694	1.95%
Opt. BUT $\alpha_{\text{CE}} = 5$	$1.03 \times 10^{-5}$	10042	3739	0.99%
Opt. BUT $q_{\text{crit}}$ fiducial	$1.72 \times 10^{-5}$	11782	5635	1.79%
Opt. BUT $Z$ fiducial	$8.79 \times 10^{-6}$	4848	2786	1.47%
Opt. BUT $\kappa$ fiducial	$7.57 \times 10^{-6}$	3625	1878	1.94%
Opt. BUT $f_{\text{b}}$ fiducial	$2.02 \times 10^{-6}$	5574	1070	0.38%
Opt. BUT $\alpha_{\text{CE}}$ fiducial	$3.72 \times 10^{-7}$	683	180	0.38%
Opt. BUT $\sigma_{\text{kick}}$ fiducial	$1.47 \times 10^{-7}$	226	63	0.56%
Opt. BUT bimodal kick	$1.24 \times 10^{-7}$	119	48	0.54%
Opt. BUT $\sigma_{\text{kick}}, \alpha_{\text{CE}}, f_{\text{b}}$ fiducial	$8.93 \times 10^{-9}$	109	5	0.04%
Opt. BUT $\kappa, \pi, Z$ fiducial	$4.12 \times 10^{-6}$	1868	1092	2.19%
Opt. BUT $\kappa, \pi, Z, f_{\text{b}}$ fiducial	$3.30 \times 10^{-7}$	611	147	0.83%
Opt. BUT $\kappa, \pi, Z, \alpha_{\text{CE}}$ fiducial	$1.90 \times 10^{-7}$	76	35	0.25%
Opt. BUT $\kappa, \pi, Z, \sigma_{\text{kick}}$ fiducial	$8.44 \times 10^{-8}$	59	27	0.87%

These results are useful in assessing which physical parameters and assumptions in our binary synthesis models most strongly affect the rate of high-velocity ejections. Keeping the notation of R19, we also include for reference the fraction  $f_{15}^{\text{RW}}$  of all  $M > 15 M_{\odot}$  stars predicted by each simulation to be runaway stars ( $v_{\text{ej}} \geq 400 \text{ km s}^{-1}$ ), properly accounting for the per-system probability and the duration of each evolutionary stage. This cut at  $15 M_{\odot}$  corresponds roughly to O-type stars and makes  $f_{15}^{\text{RW}}$  a useful prediction against which to compare observations of massive Galactic runaways. In agreement with R19 we find that  $f_{15}^{\text{RW}}$  is robust

against model variations and is limited to a few % or lower. We defer a deeper discussion of O-type runaway fractions to Sec. 5.2.

From Table 4, it is clear that the frequency of fast star ejections is governed by only a few parameters. Setting the RLOF angular momentum loss parameter  $\gamma$  or the RLOF mass transfer efficiency  $\beta_{\text{RLOF}}$  back to their fiducial values does not significantly change the probability for a companion to be ejected at a high velocity. The initial stellar properties, instead, are somewhat responsible for producing high velocity ejections. Notice that a reversion to our fiducial prescrip-

tion for the ZAMS period power law slope ( $\pi = -0.55$  for  $M_1 > 15 M_\odot$ ) actually *increases* the probability to eject fast companions relative to the optimized simulation ( $\pi = -1$  for all  $M_1$ ). This is perhaps counter-intuitive, as the steeper  $P_{\text{ZAMS}}$  slope in the optimized simulation should result in a larger probability for the low- $P_{\text{ZAMS}}$ , high- $v_{\text{orb}}$  systems most likely to eject fast companions. However, it also significantly increases the probability of the  $P_{\text{ZAMS}} \lesssim 10$  day systems most likely to undergo a merger (see Sec. 4.1). Thus the slightly shallower  $P_{\text{ZAMS}}$  log-slope provided by the fiducial prescription ends up being more effective at encouraging the low- $P_{\text{ZAMS}}$  HRS progenitor systems while not over-producing merging systems. Replacing our optimized  $P_{\text{ZAMS}}$  prescription with the fiducial prescription in the optimized simulation and all ‘Opt. BUT’ simulations does not change the qualitative results of this study.

Two other stellar initial condition parameters which affect the probability of a fast ejection are the ZAMS mass ratio distribution slope  $\kappa$  and total stellar metallicity  $Z$ . Increasing the total stellar metallicity back to its fiducial value of  $Z = 0.02$  decreases  $N_{\text{f,obs}}$  by 50% relative to the optimized simulation and returning  $\kappa$  from its optimized value of -1 to its fiducial value of 0 reduces the expected number of observable fast stars by 66%.

The most impactful parameters controlling the prevalence of high-velocity ejections are the prescriptions for common envelope evolution and post-CC natal kicks. A phase of common envelope evolution appears indeed to be a necessary phase in the evolution of binaries that produce fast ejections: with the efficiency  $\alpha_{\text{CE}}$  set back to its fiducial value of unity,  $N_{\text{f,obs}}$  is reduced by 97%. Setting  $\alpha_{\text{CE}}$  to 5 reduces  $N_{\text{f,obs}}$  by 33%. This implies that the number of observable HRS  $N_{\text{f,obs}}$  either a) increases monotonically with  $\alpha_{\text{CE}}$  up to and possibly beyond  $\alpha_{\text{CE}}=10$ , or b) peaks somewhere in the range  $5 < \alpha_{\text{CE}} < 10$ . The distinction between these cases is of little consequence, both in terms of the impact on our results and the feasibility of having an  $\alpha_{\text{CE}}$  significantly above 1 for a large population of CE systems (see Sec. 5.1.2). Note however, that  $q_{\text{crit}}$  – also related to the CE evolution – does not significantly affect  $N_{\text{f,now}}$  when set back to its fiducial donor-dependent value (see Table 1). This is because systems capable of ejecting a main sequence companion at  $v_{\text{ej}} \geq 400 \text{ km s}^{-1}$  are already biased towards small mass ratios to maximize the orbital velocity of the companion. 94% of systems ejecting a companion at  $v_{\text{ej}} \geq 400 \text{ km s}^{-1}$  in the optimized simulation have an initial  $q < 0.4$ .

With the natal kick dispersion  $\sigma_{\text{kick}}$  set back to its fiducial value of  $265 \text{ km s}^{-1}$  (but fallback fractions still set to zero),  $N_{\text{f,obs}}$  decreases by 99% relative to the optimized simulation. Implementing the double-peaked Maxwellian natal kick distribution described in Sec. 2.3 decreases  $N_{\text{f,obs}}$  by a similar amount. Mediating the natal kicks by returning to the F12 prescription for ejecta fallback fractions decreases  $N_{\text{f,obs}}$  by 81%. Together, these results demonstrate the relevance of black hole kicks for fast ejections of companions – black holes constitute 96% of the remnants left behind by CC events in systems ejecting a companion at  $v_{\text{ej}} \geq 400 \text{ km s}^{-1}$  in the optimized simulation. Only 8% of such systems would be unbound due to mass loss alone at CC (see Blaauw 1961) – significant natal kicks are required. The F12 prescription in the fiducial simulation assumes large fallback fractions for black holes and thus very small natal

kicks. We note, however, that as long as the natal kick delivered to the remnant is large, our main results are agnostic towards the nature of the remnant (see also Sec. 5.1.3.)

Small ZAMS mass ratios allow for larger companion orbital velocities and low stellar metallicities result in small stellar radii and therefore tighter orbits, but these contributions are minor when compared to the role of natal kicks and CE evolution. Included in Table 4 is a simulation with  $\sigma_{\text{kick}}$ ,  $\alpha_{\text{CE}}$  and  $f_b$  reset to their fiducial prescriptions. Relative to the optimized simulation, the number  $N_{\text{f,obs}}$  of  $t_{\text{flight}} < 100 \text{ Myr}$  stars observable in the sky is reduced by over 99.9% and clearly demonstrates the importance of these parameters. The impact of natal kicks and CE evolution is also independent of  $\kappa$ ,  $\pi$  and  $Z$ . We include in Table 4 a simulation with all of  $\kappa$ ,  $\pi$  and  $Z$  set to their fiducial values. Relative to this simulation, additionally returning  $\alpha_{\text{CE}}$ ,  $f_b$  or  $\sigma_{\text{kick}}$  to their fiducial prescriptions still results in a massive reduction in the number of companions ejected with  $v_{\text{ej}} \geq 400 \text{ km s}^{-1}$ . Note as well that the ‘Opt. BUT  $\alpha_{\text{CE}}$  fiducial’ and ‘Opt. BUT  $\sigma_{\text{kick}}$  fiducial’ simulations predict a number of  $t_{\text{flight}} < 100 \text{ Myr}$  hyper-runaway stars similar to our sample of 15 observed HRS candidates, and are thus not likely to be consistent with observations when accounting for completion and sky coverage limits. This indicates that *all* of  $\alpha_{\text{CE}}$ ,  $\sigma_{\text{kick}}$  and  $f_b$  must be set significantly far from their fiducial prescriptions for the BSS to be consistent with current observations, as any single one set individually to its fiducial value is inconsistent.

#### 4.1 The properties of progenitor binaries to fast ejections

The results presented above motivate the following picture for the production of an HRS through isolated binary evolution. Massive binaries with quite unequal mass ratios achieve small pre-CC orbital periods via CE evolution. As a result, the companion to obtains a very high pre-CC orbital velocity. RLOF does not appear to play a role for the formation of HRS. In the majority of cases, the binary also has an unequal pre-CC mass ratio, with the dying star massive than its companion. This results in the latter having a larger orbital velocity that can more easily exceed our  $400 \text{ km s}^{-1}$  cut. The massive primaries undergo core-collapse events, most often leaving black hole remnants. Subsequently, strong natal kicks are required to disrupt the binaries. The main sequence companion is then ejected with a velocity similar to its pre-CC orbital velocity.

In Fig. 4 we illustrate the importance of tight binary orbits. In this plot we show how binaries in both the fiducial (left) and optimized (right) simulations populate the period pre-CC vs. the period at ZAMS plane. By the time of the first CC event, systems above the solid white line have had their orbits widened, generally via mass loss from stellar winds for large  $P_{\text{ZAMS}}$  and wind mass loss plus RLOF at shorter  $P_{\text{ZAMS}}$ . Systems below the solid line have experienced orbital tightening, mainly via common envelope evolution. Systems at  $P_{\text{preCC}} = 0$  in this figure have merged prior to the first CC event. The contours in the right panel show the distribution only for systems which eject a companion at  $v_{\text{ej}} \geq 400 \text{ km s}^{-1}$ . These systems have periods of  $\sim 10^1 - 10^2$  days at ZAMS and experience aggressive orbital shrinking due to common envelope evolution, reducing their



orbital periods to  $\sim 1$  day. Conversely, the  $10 \lesssim P_{\text{ZAMS}} \lesssim 100$  day systems in the fiducial simulation (left panel) either experience orbital widening or have their orbits shrunk to the point of coalescence and experience a merger. Regardless, it is clear that the fiducial model does not possess the same reservoir of  $P_{\text{preCC}} \sim 1$  day systems from which to eject companions at large velocities.

As the common envelope efficiency  $\alpha_{\text{CE}}$  is increased, less orbital inspiral is required to fully eject the common envelope. It may seem counter-intuitive, then, to increase  $\alpha_{\text{CE}}$  in the optimized simulation, as it results in wider post-CE systems. In this study we are concerned with the very high tail of the velocity distribution of ejected companions, ejected from systems which may have otherwise merged if  $\alpha_{\text{CE}}$  were set lower. The priority for setting the common envelope efficiency in the optimized simulation is allowing systems to tighten while avoiding a merger. This is clear in Fig. 4, where systems at much higher  $P_{\text{ZAMS}}$  experience a merger in the fiducial simulation than in the optimized simulation.

To further demonstrate the conditions and evolutionary stages required for an HRS ejection via the BSS mechanism, we present in Fig. 5 a schematic outlining the evolution of the most common HRS progenitor system in the optimized simulation. Weighting by the per-system probabilities and the remaining lifetimes of ejected hyper-runaway companions, at ZAMS (phase A) the typical binary consists of a massive ( $M_1 \sim 27^{+14}_{-10} M_{\odot}$ ) primary and comparatively less massive ( $M_2 \sim 3.2^{+2.2}_{-1.3} M_{\odot}$ ) companion on a short-period orbit ( $P_{\text{ZAMS}} \sim 47^{+40}_{-18}$  days). When the primary star first fills its Roche lobe (phase B), the companion cannot accept the material lost from the primary and the system enters a phase of common-envelope evolution. Dynamical friction within the common envelope tightens the binary, decreasing the orbital period to  $P_{\text{preCC}} \sim 0.72^{+0.51}_{-0.21}$  days. The envelope is eventually ejected and the core of the primary is exposed as either a naked helium-burning main sequence star or naked helium-burning Hertzsprung gap star (phase C). At this time, the orbital velocity of the companion is already quite high ( $v_{\text{orb}} \sim 370^{+50}_{-60} \text{ km s}^{-1}$ ). When the primary undergoes a core-collapse event (phase D), the natal kick delivered to the remnant black hole is very large ( $v_{\text{kick}} \sim 1700^{+600}_{-500} \text{ km s}^{-1}$ ). This kick is sufficient to ionize the binary (phase E) - the companion is ejected with a velocity comparable to its pre-CC orbital velocity ( $v_{\text{ej}} \sim 445^{+87}_{-35} \text{ km s}^{-1}$ ) while the BH is ejected at an even larger velocity, ( $v_{\text{ej}} \sim 1500^{+700}_{-500} \text{ km s}^{-1}$ ).

## 5 DISCUSSION

We have shown in the previous section that the binary supernova scenario is unlikely to contribute significantly to the current population of observed HRS candidates, not unless the model prescriptions for a number of parameters are altered significantly from our fiducial prescriptions. In this section we determine whether these alterations are consistent with current understanding. To offer extra constraints on our models, we explore the predictions our fiducial and optimized models give for the number and kinematics of  $v_{\text{ej}} > 30 \text{ km s}^{-1}$  runaway stars and of binaries that remain bound following the core-collapse of the primary. Finally we

explore alternative mechanisms that may contribute to the existing population of Milky Way HRS candidates.

### 5.1 Binary evolution parameters that have the largest impact

We demonstrate in the previous section that the abundance of HRSs ejected through the BSS depends intimately on prescriptions for remnant formation (natal kick and ejecta fallback fractions), common envelope evolution, and (to a lesser extent) the binary initial mass ratio distribution and stellar metallicity. In this subsection, we explore existing constraints on each of these prescriptions from the literature, assessing whether the altered prescriptions we assume in the optimized model are consistent – or at least not in conflict – with the current understanding of stellar binary evolution. We discuss the relevant parameters in ‘chronological’ order in the life of an evolving binary (see Fig. 5).

#### 5.1.1 Initial conditions: the stellar metallicity and binary initial mass ratio

Of the relevant parameters we discuss here, a less impactful parameter which affects the frequency of  $v_{\text{ej}} \geq 400 \text{ km s}^{-1}$  companions is  $\kappa$ , the slope of the ZAMS mass ratio distribution. Though progress has been made in the past decade, attempts at constraining  $\kappa$  for massive binaries remain hamstrung by the difficulty of detecting even intermediate-mass companions around massive stars (see e.g. [Kobulnicky & Fryer 2007](#); [Duchêne & Kraus 2013](#)). Our fiducial model adopts a flat distribution, i.e.  $\kappa = 0$ , consistent with observations of nearby Galactic O-type binaries ([Sana et al. 2012](#)) and O-type binaries in the Cygnus OB2 association ([Kobulnicky et al. 2014](#)). However, our choice of  $\kappa = -1$  in the optimized simulation is also supported by several recent studies. [Sana et al. \(2013\)](#) investigate O-type binaries in the VLT-FLAMES Tarantula Survey of the 30 Doradus region in the LMC ([Evans et al. 2011](#)) and derive  $\kappa = -1.0 \pm 0.4$ . Though they alter the functional form to allow for an excess of near-equal mass binaries, [Moe & Stefano \(2013\)](#) derive  $\kappa \approx -1$  in the Milky Way, SMC and LMC when studying eclipsing O- and B-type binaries found in the *Hipparcos* ([Lefèvre et al. 2009](#)), OGLE-II ([Wyrzykowski et al. 2004](#)) and OGLE-III ([Graczyk et al. 2011](#)) data sets, respectively, though uncertainties remain large except in the case of the LMC. Even steeper mass ratio distributions have been determined by e.g. [Dunstall et al. \(2015\)](#), who investigate B-type binaries in the VLT-FLAMES Tarantula Survey and fit a mass ratio distribution with a slope  $\kappa = -2.8 \pm 0.8$ . Therefore while our choice of  $\kappa = -1$  in the optimized simulation is reasonable, larger and more complete samples are required to determine whether this accurately describes massive binary systems in the Milky Way.

The initial stellar metallicity also affects the frequency of HRS ejections. The effect of metallicity should not be overlooked, as evidence already exists of metal-poor stars ejected from the edge of the Milky Way disc ([HD 271791](#); [Heber et al. 2008b](#); [Przybilla et al. 2008b](#)). The total stellar metallicity in our fiducial simulation for all stars is the canonical Solar metallicity  $Z = 0.02$  ([Anders & Grevesse 1989](#)) and one-half dex lower ( $Z = 0.0063$ ) in our optimized simulation. While our fiducial  $Z$  is slightly higher than

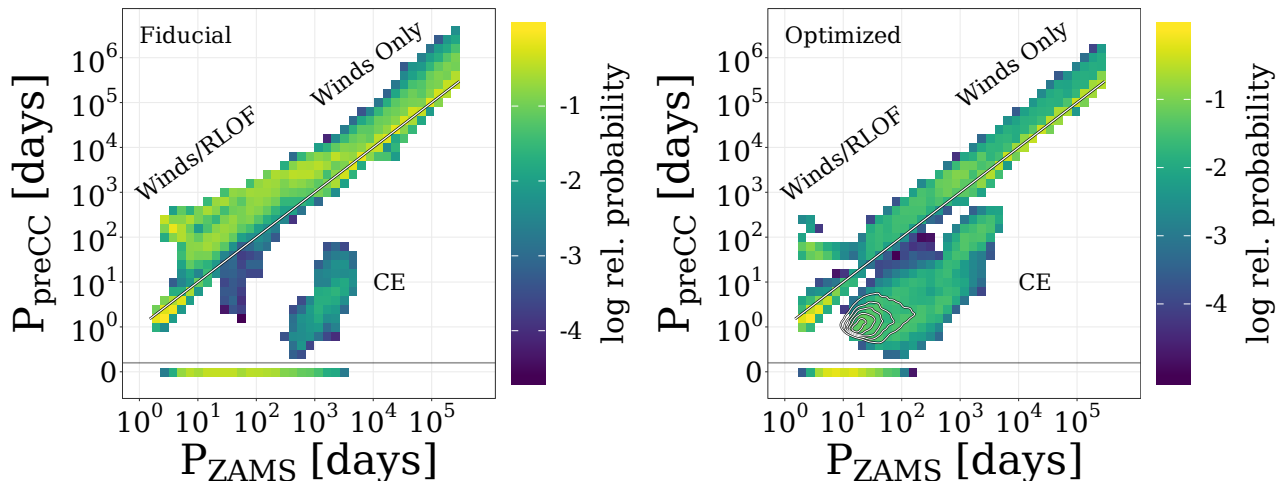


**Figure 4.** Distribution in the pre-core collapse period  $P_{\text{preCC}}$  vs. zero age main sequence period  $P_{\text{ZAMS}}$  plane for binary systems in the fiducial (left) and optimised (right) simulations. Bins are coloured by the total probability of all systems within the bin, scaled relative to the most likely bin. Solid white line shows a 1:1 correspondence. Systems lying above the white line experience orbital widening via wind mass loss or Roche lobe overflow mass transfer. Systems below the line experience orbital tightening through common envelope evolution. Systems at  $P_{\text{preCC}} = 0$  are systems that undergo a merger before the first core collapse event. White contours in the right panel show the 10%/30%/50%/70%/90% contours of the distribution of systems that eject companions at  $v_{\text{ej}} \geq 400 \text{ km s}^{-1}$

modern estimates (see [Asplund et al. 2009](#), and references therein), the Sun does not appear to have an atypical metallicity when compared to other G dwarfs ([Fuhrmann 2008](#); [Holmberg et al. 2009](#)) or B stars ([Przybilla et al. 2008c](#)) in the Solar Neighbourhood. Additionally, moderately-massive binary systems ejecting fast companions in the recent past would be expected to be more metal-rich than the Sun if anything, due to chemical enrichment over the past 4.5 Gyr. In light of this, assuming a metallicity of  $Z = 0.0063$  over the entire Milky Way is difficult to justify. However, pockets of low metallicity in the Milky Way could contribute significantly to our current observed sample of HRS candidates. Additionally, the negative radial metallicity gradient of the Milky Way should not be neglected – although the stellar density drops off towards the edge of the disc, the stellar metallicity may reach more than 0.5 dex below Solar by the edge of the disc (see [Lemasle et al. 2018](#), and references therein).

#### 5.1.2 Late-stage evolution: the common envelope efficiency

More impactful than the ZAMS mass ratio or stellar metallicity, an important physical parameter that governs the predicted number of HRSs is the common envelope efficiency  $\alpha_{\text{CE}}$ . [R19](#) found that this has little impact on the bulk population and kinematics of runaways from the BSS considering all  $v_{\text{ej}} \geq 30 \text{ km s}^{-1}$  companions, since common envelope episodes are rather rare events in massive binary evolution (at least in comparison to stable RLOF mass transfer). However, here we focus on a rare outcome of massive binary evolution – the ejection of a companion at very large velocity. Therefore, a rare evolutionary channel can (and in this case does) play a large role in the formation scenario of the outcome of interest. To eject enough companions at large velocities to be consistent with current observations, we have

shown that a common envelope efficiency significantly larger than unity must be prescribed, i.e. on top of the liberated orbital energy, other energy sources must be tapped to assist in ejecting the common envelope. These extra sources may include thermal energy and recombination within the envelope (e.g. [Han et al. 2002](#); [Webbink 2008](#); [Ivanova et al. 2013a](#)), the enthalpy of the envelope ([Ivanova & Chaichenets 2011](#)) or nuclear fusion ([Ivanova 2002](#); [Podsiadlowski et al. 2010](#)). Due to our presently-insufficient understanding of the physics involved in the common envelope phase,  $\alpha_{\text{CE}}$  is poorly-constrained and likely differs from system to system as the relevant timescales and energy sinks and sources vary (see [Regös & Tout 1995](#); [Zorotovic et al. 2010](#); [Ivanova et al. 2013a](#)). Estimates for  $\alpha_{\text{CE}}$  must be inferred from either observations of individual post-CE systems (e.g. [Afşar & Ibanoglu 2008](#); [Zorotovic et al. 2010](#)), via binary population synthesis simulations (see [Zuo & Li 2014](#), and references therein) or from detailed hydrodynamical simulations of individual systems (e.g. [Sandquist et al. 1998](#); [De Marco et al. 2011](#); [Ohlmann et al. 2016](#); [Fragos et al. 2019](#)). While sample sizes remain low, several studies (e.g. [Zorotovic et al. 2010](#); [De Marco et al. 2011](#); [Davis et al. 2012](#)) identify systems where  $\alpha_{\text{CE}} > 1$ . The  $\alpha_{\text{CE}} \gg 1$  binary progenitors of HRSs however are rare systems, and observations of much more common systems may be only partially relevant. Whether  $\alpha_{\text{CE}} = 10$  is possible in a rare and specific number of instances throughout the history of the Galaxy is currently observationally and theoretically unclear.

#### 5.1.3 The end: CC natal kicks

Among all the physical parameters we explore, the post-CC natal kick and its mediation by ejecta fallback is most influential on the frequency of hyper-runaway ejections by the BSS. We find in our optimized simulation that the primaries of HRS progenitor binaries nearly always leave a black hole

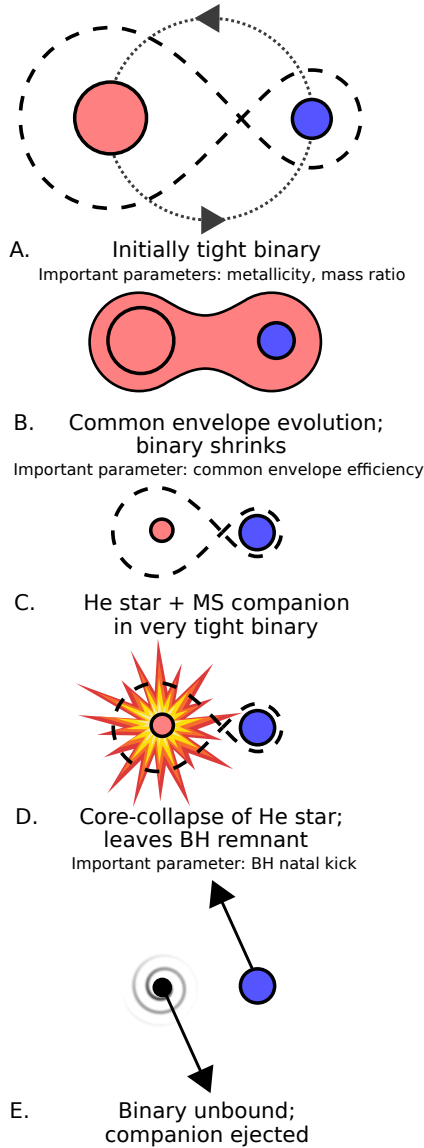


**Figure 5.** Schematic depicting the evolution of a typical system in the optimized simulation which ejects an HRS. An unequal-mass binary has a short period at zero age main sequence. Once the massive primary fills its Roche lobe, the system enters a common envelope phase, further tightening the orbit and increasing the velocity of the companion. When the primary explodes in a core-collapse supernova, the natal kick applied to the remnant black hole is strong enough to ionize the binary. The companion is ejected with a speed comparable to its pre-CC orbital velocity.

remnant according to the F12 rapid supernova algorithm. This is an effect of HRS progenitor binaries maximizing the orbital velocity of the companion, trending towards large total masses and small mass ratios. Primaries in these progenitor binaries will almost certainly be massive enough to leave a BH remnant in the F12 rapid supernova algorithm. Our fiducial treatment for the natal kick distribution for all remnants, however, is based not on BHs but on pulsar velocities. It follows Hobbs et al. (2005) who infer the distribution of 3D velocities for a sample of young (and therefore relatively unaffected by the Galactic potential) pulsars and fit a Maxwellian distribution with a root mean

squared dispersion  $\sigma_{\text{kick}} = 265 \text{ km s}^{-1}$  (see also Lyne & Lorimer 1994). The magnitudes of black hole natal kicks are poorly-constrained when compared to pulsars (e.g. Repetto et al. 2012; Janka 2013; Mandel 2016; Janka 2017; Renzo et al. 2019b) – single BHs can only be detected via microlensing of background sources (Wyrzykowski et al. 2016; Wyrzykowski & Mandel 2020) or accretion from the ISM (e.g. Fender et al. 2013; Gaggero et al. 2017). It is generally accepted that black hole natal kicks are smaller in magnitude than pulsar natal kicks (see Janka 2017; Atri et al. 2019; Chan et al. 2020). The  $\sigma_{\text{kick}} = 265 \text{ km s}^{-1}$  kick distribution for pulsars may already overestimate kick velocities, as several studies both theoretical and observational favour a double-peaked Maxwellian distribution with an additional low-velocity peak with  $\sigma_{\text{kick}} = 30 \text{ km s}^{-1}$  (e.g. Arzoumanian et al. 2002; Verbunt et al. 2017; Verbunt & Cator 2017; Vigna-Gómez et al. 2018). In the fiducial model the natal kick is then mediated by the fallback of supernova ejecta as prescribed in Eq. 16 of F12, i.e.  $v_{\text{kick}} \rightarrow v_{\text{kick}}(1 - f_b)$ , where  $f_b$  is the fallback fraction. Our fiducial feedback prescription assumes large fallback fractions for BHs, therefore very small natal kicks effectively indistinguishable from zero (R19).

While a paucity of single BH observations continues to hamstring efforts to constrain BH natal kicks, surviving binaries containing a BH can offer some insight, at least on lower-velocity kicks insufficient to ionize the binaries. Evidence for non-zero BH kicks can be found in the abundance of nearby black hole X-ray binaries (BHXRBS; Vanbeveren et al. 2020) as well as their Galactic latitude distribution and velocity distribution (Repetto et al. 2012; Repetto & Nelemans 2015; Repetto et al. 2017), in particular the peculiar velocities of certain BHXRBS, e.g. GRO 1655-40 (Willems et al. 2005), XTE J1118+480 (Fragos et al. 2009) and GS 1354-64 (Atri et al. 2019). While at least some BHXRBS may have experienced kicks similar in magnitude to pulsars, recent works find BH kicks significantly larger than  $\sim 100 \text{ km s}^{-1}$  are not required to explain current BHXRBS observations (e.g. Zuo 2015; Mandel 2016; Atri et al. 2019). Detailed 3D simulations of core-collapse supernovae accounting for the effects of ejecta fallback find that kicks  $\sim 100 \text{ km s}^{-1}$  are possible in specific and somewhat fine-tuned fallback scenarios (Chan et al. 2018; Chan et al. 2020), but favor more modest kicks in general. Naturally, systems which have experienced kicks strong enough to unbind the binary will of course not be visible as BHXRBS, therefore stronger kicks are not precluded by these studies. We explore in Sec. 5.2 whether comparing the velocities of BH-MS binaries in our simulations which remain bound post-CC to known BHXRBS can offer useful model constraints.

Additional constraints on BH natal kicks will improve with the determination of the mass distribution of runaway stars (e.g., R19, and especially runaway Wolf-Rayet stars, Dray et al. 2005) and further gravitational wave detections of binary black hole mergers (O’Shaughnessy et al. 2017; Wysocki et al. 2018). In the isolated binary scenario, non-zero BH kicks must be invoked to explain the misalignment between the orbital plane of the BH binary and the spin of the more massive companion (e.g. Kalogera 2000; O’Shaughnessy et al. 2017), which is encoded into the gravitational wave signal. On the other hand, the BH natal kick

is bounded from above by binary BH merger rates and the mass distribution of runaway stars. Strong BH kicks would often disrupt massive binaries, skewing the mass distribution of runaways towards higher masses (R19) and sharply reducing coalescence rates for binary BHs from isolated binary evolution (e.g. Belczynski et al. 2002, 2016b). For a review of the formation and evolution of isolated compact object binaries, see Postnov & Yungelson (2014). The contribution of BH binaries formed not through isolated binary evolution but via dynamical assembly in dense stellar environments must be considered as well (see Benacquista & Downing 2013). On the basis of the observed LIGO binary BH merger rate, Wysocki et al. (2018) disfavor a BH natal kick distribution with  $\sigma_{\text{kick}} \gtrsim 200 \text{ km s}^{-1}$  (see also Belczynski et al. 2016a). To conclude, while the natal kick prescriptions we assume in the optimized model cannot be directly ruled out due to a lack of observations of isolated single BHs, indirect evidence from pulsar kicks, BH XRB kinematics and BH-BH mergers generally do not offer support for this scenario.

We note here that the ‘explodability’ of massive stars and the connection between supernova progenitors and the remnants (BH or NS) they leave behind is an open question (see O’Connor & Ott 2011; Ugliano et al. 2012; Sukhbold et al. 2016; Ebinger et al. 2019; Ertl et al. 2020). While the vast majority of primaries in HRS progenitor binaries leave black hole remnants in the F12 rapid algorithm, alternative treatments could prescribe a significant proportion of NS remnants and/or a different remnant mass function (e.g. Mandel & Müller 2020). However, overall our qualitative main results – i.e. that strong remnant natal kicks and  $\alpha_{\text{CE}} \gg 1$  are required for the BSS to be a significant HRS ejection mechanism – are agnostic to the specific details of the post-SNe treatment applied to the primary. See e.g. Vanbeveren et al. (2020), who argue that the compact remnants of Wolf-Rayet (WR) stars in WR-OB star binaries receive large natal kicks regardless of whether these remnants are NSs or BHs – otherwise wind-fed high-mass XRBs would be overabundant in the Solar Neighbourhood.

The core-collapse of a massive star can in principle disrupt the binary without a significant natal kick in the case of large amounts of (fast) mass loss – for a perfectly symmetric explosion in the reference frame of the exploding star, a disruption can occur if more than half of the total mass of the binary is ejected (Blaauw 1961). While this case is rare for the typical initial period distribution of massive binaries and produces disruptions only in 16 % of the binaries avoiding merger in the fiducial simulation (R19), it might remain relevant for systems with extreme initial mass ratios. We return to this issue in Sec. 5.3.

## 5.2 Beyond HRS: Broader Implications of Model Variations

The binary evolution model variations we assume in this work impact not only the ejection rate of HRSs in general, but leave an imprint on other observables. In particular, the binaries in our simulations which remain bound post-CC can offer model constraints when compared to observations, as can the population of ejected stars with more moderate velocities ( $v_{\text{ej}} > 30 \text{ km s}^{-1}$ ). In this subsection we remark on these populations.

### 5.2.1 On surviving binaries

We discussed in Sec. 5.1.3 how BH natal kicks can be constrained by BHXRBs and BH-BH mergers. Since we do not model X-ray emission via accretion and do not follow our systems beyond the first CC event, our systems cannot directly offer predictions for BHXRB and binary black hole populations. However, we can make inferences based on the abundance and kinematics of BH-MS binaries in our simulation which remain bound after the first CC. Even if they are not disrupted, the natal kick and the change in gravitational potential due to mass loss from the primary can impart peculiar velocities to these systems, possibly up to and exceeding runaway ( $v_{\text{ej}} > 30 \text{ km s}^{-1}$ ) velocities (van Oijen 1989). In the case of Hercules X-1, a pulsar XRB at high Galactic latitude, Sutantyo (1975) shows that the spherically-symmetric (i.e.  $v_{\text{kick}} \sim 0$ ) explosion of a  $\sim 4 M_{\odot}$  helium star in orbit with a  $\sim 2 M_{\odot}$  companion can explain its quite high ejection velocity ( $v_{\text{ej}} \sim 150 \text{ km s}^{-1}$ ). Runaway stars still in orbit with a compact remnant could be identified as single-line (SB1) spectroscopic binaries. If the orbits are sufficiently tight to allow the black hole remnant to eventually accrete material from the companion, these systems may become visible as BHXRBs.

In the fiducial simulation, 6.7 % of systems remain bound as BH-MS binaries after the first CC event. Our simulations predict the systemic velocity  $v_{\text{sys}}$  imparted to these systems, here defined as the velocity of the centre of mass of the post-CC BH-MS binary in the frame of reference of its pre-CC centre of mass (Kalogera 1996; Tauris & Takens 1998). In agreement with R19 (c.f. Fig. 11) we find that  $\sim 80$  % of the BH-MS systems in the fiducial simulation acquire  $v_{\text{sys}} \simeq 0 \text{ km s}^{-1}$ . This is due to our fiducial prescription for post-CC ejecta fallback following F12 – many BH progenitors experience complete ejecta fallback; the remnant experiences no kick at all and no mass is lost from the system. Only 4 % of the BH-MS binaries in our fiducial simulation achieve systemic velocities in excess of  $30 \text{ km s}^{-1}$ .

The optimized simulation, on the other hand, includes very different prescriptions for BH natal kicks and ejecta fallback, and therefore predicts a very different velocity distribution for surviving BH-MS binaries. Owing to the large disruption fraction, only 0.5 % of systems in the optimized simulation remain bound as a BH-MS binary after the first CC event. Of these, however, 99.9 % achieve  $v_{\text{sys}} > 30 \text{ km s}^{-1}$  (see Fig. A1). This, combined with the fact that 95 % have post-CC separations below  $300 R_{\odot}$ , indicate the optimized simulation would predict runaway BHXRBs to be quite common. In fact, 45 % of BH-MS binaries achieve hyper-runaway speeds,  $v_{\text{sys}} \geq 400 \text{ km s}^{-1}$ . The optimized simulation predicts that lone hyper-runaway stars outnumber hyper-runaway stars with BH companions by only a factor of 1.4. To date, no hyper-runaway BHXRBs or SB1 binaries have been observed. With a sample of 16 known BHXRBs, Atri et al. (2019) find no BHXRBs that intersect the Galactic disc with a peculiar velocity above  $\sim 200 \text{ km s}^{-1}$ ; a systemic velocity achieved by 83 % of the BH-MS binaries in the optimized simulation. This absence of high-velocity BHXRBs or SB1 systems disfavours our optimized model. It is worth mentioning, however, that without accounting for deceleration by the Galactic potential, BH-MS binaries in our optimized simulation travel for  $\sim 17 \text{ kpc}$  on average from their



birth locations before the companion star leaves the main sequence. At such distances any X-ray emission may be difficult to detect and BHXRB samples would therefore be biased towards low- $v_{\text{sys}}$  systems remaining at low Galactic latitude.

Systems that remain bound after the first CC are unlikely to be disrupted by the eventual CC of the remaining MS companion (e.g., O’Shaughnessy et al. 2017) provided they do not merge beforehand. If the separation is sufficiently small, the resulting BH-BH binary may eventually become a gravitational wave source. Since we do not follow the evolution of our binary systems beyond the first CC event, our simulations cannot provide predictions for gravitational waves merger rates. However, from the different binary disruption fractions it is clear that the fiducial and optimized simulations would give quite different predictions for the rate and characteristics of BH-BH mergers. Therefore, upcoming statistical samples of BH-BH mergers will provide model constraints, albeit from a different part of the parameter space than what is relevant for the formation of hyper-runaway stars (see previous Section).

### 5.2.2 On massive runaway stars

Naturally, the model variations we explore here to encourage the ejection of HRSs also strongly influence the fraction of systems which eject companions at  $30 \text{ km s}^{-1} < v_{\text{ej}} < 400 \text{ km s}^{-1}$  and the velocity distribution of these ‘runaway’ stars. Properly accounting for initial configuration probabilities and the duration of each evolutionary phase, the fiducial simulation predicts that in total, 0.54% of all O-type ( $M \gtrsim 15 M_{\odot}$ ) stars in the Milky Way are runaways (see Table 4). The O-type runaway fraction increases to 1.6% in the optimized simulation but never significantly exceeds  $\sim 2\%$  in any simulation presented in Table 4. Although the likelihood of hyper-runaway ejections varies by four orders of magnitude among our chosen models, the O-type runaway fraction is much more robust against model variation. This is consistent with R19 and the binary synthesis study of Eldridge et al. (2011) but in potential tension with observational findings that  $\sim 10\text{--}20\%$  of O-type stars are runaways (e.g., Blaauw 1961; Tetzlaff et al. 2011; Maíz Apellániz et al. 2018) and the suggestion of Hoogerwerf et al. (2001) that  $\sim 2/3$  of runaway stars are due to disrupted binaries (though see Jilinski et al. (2010) for a challenge to this conclusion). Unless we have overlooked other mechanisms which greatly shrink binary orbits and eject companions at runaway speeds, the inability of even our optimized simulation to match the above observations suggests that the role of the dynamical ejection scenario has been under-estimated and/or observations of O-type stars are biased towards runaways.

### 5.2.3 On neutron star kinematics

In addition to predicting large BH-MS systemic velocities that are in potential tension with observations, the optimized simulation also predicts quite large neutron star ejection velocities due to the large kicks assumed. Using 19 young (and therefore relatively unaffected by the Galactic potential) pulsars with proper motion measurements, Verbunt et al. (2017) fit the observed velocity distribution to

a double Maxwellian distribution. Their best-fit model suggests that no more than 2% of Galactic pulsars are moving at  $v > 1000 \text{ km s}^{-1}$ . In the optimized simulation, 79% of neutron stars ejected from disrupted binaries are ejected with velocities above this threshold (see Fig. A1). Although observations may be biased towards close-by, low-velocity pulsars, they nonetheless are in contrast with our optimized model.

### 5.3 Further caveats

There are caveats which should be considered when comparing the HRS populations predicted by the simulations to the current sample of observed HRS candidates.

Notice that we assume in Eq. 5 a constant Galactic star formation rate, a reasonable assumption for at least the last  $\sim 2 \text{ Gyr}$  (Snaith et al. 2014, 2015). Spatial or temporal variations in the global star formation rate in the Milky Way will affect the number of observable HRSs, especially the more massive and thus shorter-lived among these. A recent burst of star formation somewhere in the Milky Way disc will lead to an increase in runaway and hyper-runaway stars ejected from that location after a delay corresponding to at least the lifetime of the most massive stars we consider ( $\sim 3 \text{ Myr}$ , Zapartas et al. 2017). Our assumption for the global Galactic star formation rate,  $3.5 M_{\odot} \text{ yr}^{-1}$ , is a common choice for binary population synthesis studies (e.g. Dominik et al. 2012), but rather optimistic when compared to recent results converging on  $1\text{--}2 M_{\odot} \text{ yr}^{-1}$  (Chomiuk & Povich 2011; Licquia & Newman 2015, and references therein). However, replacing the star formation rate seen in Eq. 5 with a lower value will reduce all  $N_{\text{f,obs}}$  values in Table 4 by the same factor and would not qualitatively change any results presented in this study regarding the conditions and physics required to eject fast stars via the BSS mechanism. A lower star formation rate in fact strengthens our conclusion that ejecting enough fast companions to be consistent with current observations of Milky Way HRS candidates requires prescriptions for remnant natal kicks, ejecta fallback and common envelope evolution that significantly differ from our fiducial assumptions for the overall binary population.

Another consideration is our choice of lower bound on the ZAMS mass ratio distribution. In all simulations we generate only systems with  $0.1 < q_{\text{ZAMS}} < 1$ , a commonly-explored interval (e.g. Sana et al. 2012, 2013; Moe & Stefano 2013; Dunstall et al. 2015) dictated by detectability limits and the assumption that systems with  $q_{\text{ZAMS}} < 0.1$  are expected to eventually merge (e.g., de Mink et al. 2013). With the somewhat idealized physics we assume in the optimized simulation(s), however, this assumption may not necessarily hold true. Indeed, re-running the optimized simulation with a fixed companion lower mass limit of  $M_{2,\text{ZAMS}} = 0.5 M_{\odot}$  does increase the number  $N_{\text{f,obs}}$  of observable early-type HRSs by 45%, however the qualitative results presented in this study do not change. Given the observational realities of detecting secondaries around massive stars in highly unequal-mass systems (see e.g. Kobulnicky & Fryer 2007; Duchêne & Kraus 2013), it remains unclear what fraction of massive binaries have extreme  $q < 0.1$  mass ratios or whether such a subpopulation can even be realistically constrained by observations. If future observational constraints suggest a significant population of such system which avoid

mergers, further investigation on the evolution of extreme mass ratio binaries would be warranted.

As mentioned in Sec. 5.1.2, one limitation of our approach is that we assume a single value of  $\alpha_{\text{CE}}$  applies to all binaries. In reality there is more likely a distribution of values, where even optimistically only for rare systems these are equal to our optimized value to  $\alpha_{\text{CE}} = 10$ . In the optimized simulation this same caveat applies to the total stellar metallicity  $Z$  and fallback fraction  $f_b$  – we apply a single value to the entire binary population rather than allowing for multiple populations to be present as minority fractions of the broader population. A model where  $Z$  and  $\alpha_{\text{CE}}$  in particular are allowed to vary is a venue worth exploring in the future.

Finally, it is worth pointing out that the parameters chosen for our optimized simulation were chosen based on simple assumptions about their role in enhancing the number of short-period, high-orbital velocity systems. We do not fully explore the highly-dimensional space of initial conditions and binary evolution parameters to find the truly optimal set of prescriptions. Some of our assumptions may be overly simplistic, e.g. see Sec. 4 where the fiducial  $P_{\text{ZAMS}}$  prescription is in fact more effective than the “optimized” prescription at ejecting fast companions. A more complete exploration of the entire parameter space and the correlations between parameters is a possible future direction for this study.

#### 5.4 Alternative origins of hyper-runaway stars

Here we only consider main-sequence stars ejected from a disrupted binary system. If the BSS mechanism is unable to contribute significantly to the known population of Milky Way main sequence hyper-runaway candidates, which mechanism is responsible? One possible mechanism includes the dynamical ejection scenario (DES) wherein stars are ejected via three- or four-body interactions in dense clusters (Poveda et al. 1967; Leonard & Duncan 1990; Leonard 1991; Fujii & Portegies Zwart 2011; Banerjee et al. 2012). Oh & Kroupa (2016) explore the ejection of massive stars from moderately massive ( $M_{\text{cl}} \approx 3000 M_{\odot}$ ) star clusters under diverse initial conditions. Ejections in excess of  $200 \text{ km s}^{-1}$  are very rare except in the model where the cluster consists of only initially massive ( $M_1 \geq 5 M_{\odot}$ ) binaries on short, circular orbits. In a suite of similar simulations, Perets & Šubr (2012) infer a dynamical ejection rate for  $v_{\text{ej}} > 450 \text{ km s}^{-1}$  B-type HRSs from young clusters of  $\sim 10 \text{ Gyr}^{-1}$  in their most realistic model, and conclude that the DES is unlikely to contribute significantly to the Galactic population of hyper-runaway stars. Since the majority of ejections from dynamical encounters happen in the very early evolution of a cluster (e.g. Oh & Kroupa 2016), observations of the stellar dynamics in very young regions (such as the Orion Nebula Cluster, e.g., Schoettler et al. 2019, 2020, or R136 in the LMC, e.g., Lennon et al. 2018; Renzo et al. 2019a) can constrain the DES scenario, including for the rare very fast ejections.

Beyond the BSS and the classical dynamical ejection scenario, possible but less-studied scenarios have been suggested. A first potential pathway is ejections which involve three- or four-body interactions involving massive stars. Gvaramadze (2009) point out three possible ejection channels: (i) the breakup of an unstable hierarchical triple com-

posed of massive stars (inner binary of two  $\sim 50 M_{\odot}$  stars with a  $\sim 10 M_{\odot}$  outer companion, (ii) binary-binary dynamical interactions where massive stars ( $\sim 20\text{--}40 M_{\odot}$ ) compose at least one member of the binaries, and (iii) exchange encounters between hard, massive binaries and  $\gtrsim 200 M_{\odot}$  very massive stars, which form via runaway collisions of ordinary stars in the cores of young massive star clusters (Portegies Zwart & McMillan 2002). All three mechanisms are capable of ejecting massive companions far in excess of  $400 \text{ km s}^{-1}$ .

Second, encounters between stellar binaries and an intermediate-mass black hole (IMBH) in analogy to the Hills mechanism may also contribute to the population of high-velocity stars ejected from the Galactic disc or halo (Pfahl 2005; Gualandris & Portegies Zwart 2007; Hopman 2009; Sesana et al. 2012). Fragione & Gualandris (2019) assign realistic IMBH masses to the centres of Milky Way globular clusters and study the ejection of high-velocity stars. They infer a fast star ejection rate from this IMBH channel of  $\sim 10^{-4} \text{ yr}^{-1}$  with a  $v_{\text{ej}}$  distribution which peaks at  $v_{\text{ej}} \approx 300 \text{ km s}^{-1}$  with a tail extending to  $\sim 2000 \text{ km s}^{-1}$ .

Finally, we must also consider the possibility that although the backward trajectories of observed HRSs point towards the Galactic disc, they may have been born elsewhere. Main sequence HRSs originally of extragalactic origins may serendipitously intersect the Milky Way disc and appear as disc-ejected HRSs. These stars could come from the tidal disruption of infalling dwarf galaxies as suggested by (Abadi et al. 2009) or from a high-velocity ejection from the Large Magellanic Cloud (Gualandris & Portegies Zwart 2007; Przybilla et al. 2008a; Boubert & Evans 2016; Boubert et al. 2017; Erkal et al. 2019) or M31 (Sherwin et al. 2008), though none of our HRS candidates seem to point from the LMC or M31. Any or all of the above origins and mechanisms could contribute to the Galactic population of hyper-runaways.

## 6 SUMMARY AND CONCLUSION

We have performed an extensive suite of numerical simulations to ascertain the probability with which disruptions of binary systems by core-collapse supernovae are able to eject main sequence companions at large velocities ( $v_{\text{ej}} \geq 400 \text{ km s}^{-1}$ ). With each simulation we predict the number of these so-called ‘hyper-runaway stars’ (HRSs) in the Milky Way which should still be reasonably nearby with  $t_{\text{flight}} < 100 \text{ Myr}$ . We systematically vary parameters which dictate the initial conditions and physics governing the evolution of binary systems. In doing so, our aim is to rigorously test under a variety of models whether the binary supernova scenario contributes significantly to the observed population of early-type HRS candidates seemingly ejected from the Milky Way disc at high velocities. By varying parameters one-by-one, we determine which are most important when considering the ejection of companions at large velocities. Our findings can be summarized as follows:

- In our fiducial model, which generates and evolves binary systems according to free parameters chosen to be consistent with contemporary observations and theory, core-collapse supernovae in binaries do not eject companions at large velocities often enough for the binary supernova sce-

nario to contribute significantly to the known population of HRS candidates (see Fig 3).

- By varying relevant parameters one-by-one, we find that the probability of fast companion ejections depends most intimately on the common-envelope efficiency  $\alpha_{\text{CE}}$  and the parameters which dictate the magnitude of the post-CC natal kick imparted to stellar remnants, i.e. the ejecta fallback fraction  $f_b$  and natal kick distribution dispersion  $\sigma_{\text{kick}}$  (see Table 4). The  $\alpha_{\text{CE}}$  parameter indirectly governs the amount of orbital tightening – and therefore the increase in orbital velocity – that occurs during the common-envelope phase. A large orbital velocity in turn results in a greater ejection velocity for the companion if the system is disrupted. The natal kick parameters  $f_b$  and  $\sigma_{\text{kick}}$ , in turn, dictate the frequency with which binary systems are disrupted immediately following the core-collapse of the primary.

- To a lesser degree, the probability of fast companion ejection increases with decreasing total stellar metallicity and with an increasing proportion of highly-unequal initial mass ratios in the binary population. At fixed stellar mass, stars of lower stellar metallicity are smaller in radius and can therefore orbit at a smaller separation without undergoing a merger. At fixed system mass, a smaller mass ratio between the companion and primary results in a greater orbital velocity for the companion.

- While the rate of HRS ejections via the binary supernova scenario depends strongly on the above parameters, the runaway fraction ( $v_{\text{ej}} > 30 \text{ km s}^{-1}$ ) among O-type stars is robust against model variations and is limited to  $\lesssim 2\%$ .

- The prototypical progenitor binary of an HRS ejected by the binary supernova scenario is composed of a massive, unequal-mass binary on a short initial period. Upon the primary filling its Roche lobe, the system enters a phase of common envelope evolution and hardens further. The core-collapse of the primary leaves a black hole remnant, which experiences an asymmetric post-CC natal kick extreme enough to disrupt the binary. The main sequence companion escapes with an ejection velocity similar in magnitude to its pre-core collapse orbital velocity ( $v_{\text{ej}} \gtrsim 400 \text{ km s}^{-1}$ , see Figs. 3 and 5). The remnant black hole is ejected at a much larger velocity,  $v_{\text{ej}} \simeq 1700 \text{ km s}^{-1}$ .

- For a model to predict a number of  $t_{\text{flight}} < 100 \text{ Myr}$  HRSs comparable to the current observed population of HRS candidates, it is not sufficient to tune one of the aforementioned parameters in the direction which favours the ejection of fast companions. *All of* the common envelope efficiency  $\alpha_{\text{CE}}$  and the stellar remnant natal kick parameters  $f_b$  and  $\sigma_{\text{kick}}$  must be tuned in favourable directions for our population synthesis model to predict a number of hyper-runaway stars consistent with observations (see Table 4).

- To match observations, the relevant parameters above must be tuned to values or prescriptions which are improbable or disfavoured – but not ruled out – by contemporary constraints on these parameters from the literature.

From the results summarized above, we may conclude that the binary supernova scenario is unlikely to contribute significantly to the current known population of HRS candidates. This conclusion is broadly consistent with other works exploring the binary supernova scenario (e.g. [Portegies Zwart 2000](#); [Eldridge et al. 2011](#); [Renzo et al. 2019b](#)). With our detailed quantitative investigation we outline for

the first time the evolutionary path of hyper-runaway stars ejected via the binary supernova scenario and the characteristics of their binary progenitors. Future dedicated theoretical and observational works may be used to test the existence of such progenitors.

## ACKNOWLEDGEMENTS

We are grateful to the anonymous referee for their prompt and constructive feedback. We thank I. Mandel for helpful discussions, D. Hendricks, S. Jha and S. Justham for useful comments and R. Izzard for letting us use the `binary_c` code. FAE acknowledges D. Boubert and S. Kreuzer for helpful correspondence regarding the Open Fast Stars Catalog. MR acknowledges M. Heemskerk for allowing continued use of the helios cluster at the University of Amsterdam, and S. de Mink and E. Zapartas for useful discussions. FAE acknowledges funding support from the Natural Sciences and Engineering Research Council of Canada (NSERC) Post-graduate Scholarship.

## DATA AVAILABILITY

The data underlying this article are available via Zenodo at <https://dx.doi.org/10.5281/zenodo.3860055> and via the Open Fast Stars Catalog at <https://faststars.space/>

## REFERENCES

- Aarseth S. J., 1974, *A&A*, **35**, 237  
 Abadi M. G., Navarro J. F., Steinmetz M., 2009, *ApJ*, **691**, L63  
 Abolfathi B., et al., 2018, *ApJS*, **235**, 42  
 Afşar M., Ibañoğlu C., 2008, *MNRAS*, **391**, 802  
 Alam S., et al., 2015, *ApJS*, **219**, 12  
 Anders E., Grevesse N., 1989, *Geochimica Cosmochimica Acta*, **53**, 197  
 Arzoumanian Z., Chernoff D. F., Cordes J. M., 2002, *ApJ*, **568**, 289  
 Asplund M., Grevesse N., Sauval A. J., Scott P., 2009, *ARA&A*, **47**, 481  
 Atri P., et al., 2019, *MNRAS*, **489**, 3116  
 Banerjee S., Kroupa P., Oh S., 2012, *ApJ*, **746**, 15  
 Bauer E. B., White C. J., Bildsten L., 2019, *ApJ*, **887**, 68  
 Belczyński K., Bulik T., 1999, *A&A*, **346**, 91  
 Belczynski K., Kalogera V., Bulik T., 2002, *ApJ*, **572**, 407  
 Belczynski K., Holz D. E., Bulik T., O’Shaughnessy R., 2016a, *Nature*, **534**, 512  
 Belczynski K., Repetto S., Holz D. E., O’Shaughnessy R., Bulik T., Berti E., Fryer C., Dominik M., 2016b, *ApJ*, **819**, 108  
 Benacquista M. J., Downing J. M. B., 2013, *Living Reviews in Relativity*, **16**, 4  
 Blaauw A., 1961, *Bull. Astron. Inst. Netherlands*, **15**, 265  
 Bland-Hawthorn J., Gerhard O., 2016, *ARA&A*, **54**, 529  
 Boersma J., 1961, *Bull. Astron. Inst. Netherlands*, **15**, 291  
 Böker T., 2010, in de Grijs R., Lépine J. R. D., eds, *IAU Symposium Vol. 266, Star Clusters: Basic Galactic Building Blocks Throughout Time and Space*. pp 58–63 ([arXiv:0910.4863](https://arxiv.org/abs/0910.4863)), [doi:10.1017/S1743921309990871](https://doi.org/10.1017/S1743921309990871)  
 Boubert D., Evans N. W., 2016, *ApJ*, **825**, L6  
 Boubert D., Erkal D., Evans N. W., Izzard R. G., 2017, *Monthly Notices of the Royal Astronomical Society*, **469**, 2151  
 Boubert D., Guillochon J., Hawkins K., Ginsburg I., Evans N. W., Strader J., 2018, *MNRAS*, **479**, 2789  
 Bovy J., 2015, *ApJS*, **216**, 29

- Bromley B. C., Kenyon S. J., Brown W. R., Geller M. J., 2009, *ApJ*, **706**, 925
- Bromley B. C., Kenyon S. J., Geller M. J., Brown W. R., 2012, *ApJ*, **749**, L42
- Brown W. R., 2015, *ARA&A*, **53**, 15
- Brown W. R., Geller M. J., Kenyon S. J., Kurtz M. J., 2005, *ApJ*, **622**, L33
- Brown W. R., Geller M. J., Kenyon S. J., Kurtz M. J., 2006, *ApJ*, **640**, L35
- Brown W. R., Geller M. J., Kenyon S. J., Kurtz M. J., Bromley B. C., 2007, *ApJ*, **660**, 311
- Brown W. R., Geller M. J., Kenyon S. J., 2009, *ApJ*, **690**, 1639
- Brown W. R., Geller M. J., Kenyon S. J., 2012, *ApJ*, **751**, 55
- Brown W. R., Geller M. J., Kenyon S. J., 2014, *ApJ*, **787**, 89
- Brown W. R., Anderson J., Gnedin O. Y., Bond H. E., Geller M. J., Kenyon S. J., 2015, *ApJ*, **804**, 49
- Brown W. R., Lattanzi M. G., Kenyon S. J., Geller M. J., 2018, *ApJ*, **866**, 39
- Burrows A., Hayes J., 1996, *Phys. Rev. Lett.*, **76**, 352
- Burrows A., Hubbard W. B., Saumon D., Lunine J. I., 1993, *ApJ*, **406**, 158
- Capuzzo-Dolcetta R., Fragione G., 2015, *MNRAS*, **454**, 2677
- Chan C., Mäijller B., Heger A., Pakmor R., Springel V., 2018, *ApJ*, **852**, L19
- Chan C., Müller B., Heger A., 2020, *MNRAS*, **495**, 3751
- Chomiuk L., Povich M. S., 2011, *AJ*, **142**, 197
- Claeys J. S. W., Pols O. R., Izzard R. G., Vink J., Verbunt F. W. M., 2014, *A&A*, **563**, A83
- Contigiani O., Rossi E. M., Marchetti T., 2019, *MNRAS*, **487**, 4025
- Davis P. J., Kolb U., Knigge C., 2012, *MNRAS*, **419**, 287
- De Marco O., Passy J.-C., Moe M., Herwig F., Mac Low M.-M., Paxton B., 2011, *MNRAS*, **411**, 2277
- Dewi J. D. M., Tauris T. M., 2000, *A&A*, **360**, 1043
- Diehl R., et al., 2006, *Nature*, **439**, 45
- Dominik M., Belczynski K., Fryer C., Holz D. E., Berti E., Bulik T., Mandel I., O’Shaughnessy R., 2012, *ApJ*, **759**, 52
- Dray L. M., Dale J. E., Beer M. E., Napiwotzki R., King A. R., 2005, *MNRAS*, **364**, 59
- Duchêne G., Kraus A., 2013, *ARA&A*, **51**, 269
- Dunstall P. R., et al., 2015, *A&A*, **580**, A93
- Ebinger K., Curtis S., Fröhlich C., Hempel M., Perego A., Liebrandt M., Thielemann F.-K., 2019, *ApJ*, **870**, 1
- Edelmann H., Napiwotzki R., Heber U., Christlieb N., Reimers D., 2005, *ApJ*, **634**, L181
- Eldridge J. J., 2009, *MNRAS*, **400**, L20
- Eldridge J. J., Langer N., Tout C. A., 2011, *MNRAS*, **414**, 3501
- Erkal D., Boubert D., Gualandris A., Evans N. W., Antonini F., 2019, *MNRAS*, **483**, 2007
- Ertl T., Woosley S. E., Sukhbold T., Janka H. T., 2020, *ApJ*, **890**, 51
- Evans C. J., et al., 2011, *A&A*, **530**, A108
- Fender R. P., Maccarone T. J., Heywood I., 2013, *MNRAS*, **430**, 1538
- Fragione G., Capuzzo-Dolcetta R., 2016, *MNRAS*, **458**, 2596
- Fragione G., Gualandris A., 2019, *MNRAS*, **489**, 4543
- Fragos T., Willems B., Kalogera V., Ivanova N., Rockefeller G., Fryer C. L., Young P. A., 2009, *ApJ*, **697**, 1057
- Fragos T., Andrews J. J., Ramirez-Ruiz E., Meynet G., Kalogera V., Taam R. E., Zezas A., 2019, *ApJ*, **883**, L45
- Fryer C. L., Belczynski K., Wiktorowicz G., Dominik M., Kalogera V., Holz D. E., 2012, *ApJ*, **749**, 91
- Fuhrmann K., 2008, *MNRAS*, **384**, 173
- Fujii M. S., Portegies Zwart S., 2011, *Science*, **334**, 1380
- Gaggero D., Bertone G., Calore F., Connors R. M. T., Lovell M., Markoff S., Storm E., 2017, *Phys. Rev. Lett.*, **118**, 241101
- Gaia Collaboration et al., 2016, *A&A*, **595**, A2
- Gaia Collaboration et al., 2018, *A&A*, **616**, A1
- Geier S., et al., 2013, *A&A*, **554**, A54
- Geier S., et al., 2015, *Science*, **347**, 1126
- Genzel R., Eisenhauer F., Gillessen S., 2010, *Reviews of Modern Physics*, **82**, 3121
- Gnedin O. Y., Gould A., Miralda-Escudé J., Zentner A. R., 2005, *ApJ*, **634**, 344
- Graczyk D., et al., 2011, *Acta Astron.*, **61**, 103
- Gualandris A., Portegies Zwart S., 2007, *MNRAS*, **376**, L29
- Gualandris A., Portegies Zwart S., Sipior M. S., 2005, *MNRAS*, **363**, 223
- Guillochon J., Loeb A., 2015, *ApJ*, **806**, 124
- Guillochon J., Parrent J., Kelley L. Z., Margutti R., 2017, *ApJ*, **835**, 64
- Gunn J. E., Ostriker J. P., 1970, *ApJ*, **160**, 979
- Gvaramadze V. V., 2009, *MNRAS*, **395**, L85
- Han Z., Podsiadlowski P., Maxted P. F. L., Marsh T. R., Ivanova N., 2002, *MNRAS*, **336**, 449
- Hansen B. M. S., 2003, *ApJ*, **582**, 915
- Hattori K., Valluri M., Castro N., Roederer I. U., Mahler G., Khullar G., 2019, *ApJ*, **873**, N16
- Heber U., Hirsch H. A., Edelmann H., Napiwotzki R., O’Toole S. J., Brown W., Altmann M., 2008a, *Hypervelocity Stars: Young and Heavy or Old and Light?*, p. 167
- Heber U., Edelmann H., Napiwotzki R., Altmann M., Scholz R. D., 2008b, *A&A*, **483**, L21
- Hills J. G., 1988, *Nature*, **331**, 687
- Hirsch H. A., Heber U., O’Toole S. J., Bresolin F., 2005, *A&A*, **444**, L61
- Hobbs G., Lorimer D. R., Lyne A. G., Kramer M., 2005, *MNRAS*, **360**, 974
- Holland-Ashford T., Lopez L. A., Auchettl K., Temim T., Ramirez-Ruiz E., 2017, *ApJ*, **844**, 84
- Holmberg J., Nordström B., Andersen J., 2009, *A&A*, **501**, 941
- Hoogerwerf R., de Bruijne J. H. J., de Zeeuw P. T., 2001, *A&A*, **365**, 49
- Hopman C., 2009, *ApJ*, **700**, 1933
- Huang Y., et al., 2017, *ApJ*, **847**, L9
- Hurley J. R., Pols O. R., Tout C. A., 2000, *MNRAS*, **315**, 543
- Hurley J. R., Tout C. A., Pols O. R., 2002, *MNRAS*, **329**, 897
- Irrgang A., Kreuzer S., Heber U., 2018, *A&A*, **620**, A48
- Irrgang A., Geier S., Heber U., Kupfer T., Fürst F., 2019, *A&A*, **628**, L5
- Ivanova N., 2002, PhD thesis, University of Oxford
- Ivanova N., Chaichenets S., 2011, *ApJ*, **731**, L36
- Ivanova N., et al., 2013a, *A&ARv*, **21**, 59
- Ivanova N., Justham S., Avendano Nandez J. L., Lombardi J. C., 2013b, *Science*, **339**, 433
- Izzard R. G., Tout C. A., Karakas A. I., Pols O. R., 2004, *MNRAS*, **350**, 407
- Izzard R. G., Dray L. M., Karakas A. I., Lugaro M., Tout C. A., 2006, *A&A*, **460**, 565
- Izzard R. G., Glebbeek E., Stancliffe R. J., Pols O. R., 2009, *A&A*, **508**, 1359
- Janka H.-T., 2013, *MNRAS*, **434**, 1355
- Janka H.-T., 2017, *ApJ*, **837**, 84
- Janka H. T., Mueller E., 1994, *A&A*, **290**, 496
- Jilinski E., Ortega V. G., Drake N. A., de la Reza R., 2010, *ApJ*, **721**, 469
- Justham S., Wolf C., Podsiadlowski P., Han Z., 2009, *A&A*, **493**, 1081
- Kalogera V., 1996, *ApJ*, **471**, 352
- Kalogera V., 2000, *ApJ*, **541**, 319
- Katsuda S., et al., 2018, *ApJ*, **856**, 18
- Katz J. I., 1975, *Nature*, **253**, 698
- Kenyon S. J., Bromley B. C., Geller M. J., Brown W. R., 2008, *ApJ*, **680**, 312
- Kenyon S. J., Bromley B. C., Brown W. R., Geller M. J., 2014, *ApJ*, **793**, 122



- Knigge C., Coe M. J., Podsiadlowski P., 2011, *Nature*, **479**, 372
- Kobulnicky H. A., Fryer C. L., 2007, *ApJ*, **670**, 747
- Kobulnicky H. A., et al., 2014, *ApJS*, **213**, 34
- Koposov S. E., et al., 2019, *MNRAS*, p. 2680
- Kreuzer S., Irrgang A., Heber U., 2020, *A&A*, **637**, A53
- Kroupa P., 2001, *MNRAS*, **322**, 231
- Kuiper G. P., 1935, *PASP*, **47**, 15
- Lefèvre L., Marchenko S. V., Moffat A. F. J., Acker A., 2009, *A&A*, **507**, 1141
- Lemasle B., et al., 2018, *A&A*, **618**, A160
- Lennon D. J., van der Marel R. P., Ramos Lerate M., O’Mullane W., Sahlmann J., 2017, *A&A*, **603**, A75
- Lennon D. J., et al., 2018,
- Leonard P. J. T., 1991, *AJ*, **101**, 562
- Leonard P. J. T., Duncan M. J., 1990, *AJ*, **99**, 608
- Leonard P. J. T., Hills J. G., Dewey R. J., 1994, *ApJ*, **423**, L19
- Li Y.-B., et al., 2018, *AJ*, **156**, 87
- Licquia T. C., Newman J. A., 2015, *ApJ*, **806**, 96
- Liu Z.-W., Tauris T. M., Röpke F. K., Moriya T. J., Kruckow M., Stancliffe R. J., Izzard R. G., 2015, *A&A*, **584**, A11
- Luo A.-L., et al., 2016, VizieR Online Data Catalog, **5149**
- Lyne A. G., Lorimer D. R., 1994, *Nature*, **369**, 127
- Madigan A.-M., Pfuhl O., Levin Y., Gillessen S., Genzel R., Perets H. B., 2014, *ApJ*, **784**, 23
- Maíz Apellániz J., Pantaleoni González M., Barbá R. H., Simón-Díaz S., Negueruela I., Lennon D. J., Sota A., Trigueros Páez E., 2018, *A&A*, **616**, A149
- Mandel I., 2016, *MNRAS*, **456**, 578
- Mandel I., Müller B., 2020, arXiv e-prints, p. arXiv:2006.08360
- Marchetti T., Rossi E. M., Brown A. G. A., 2019, *MNRAS*, **490**, 157
- Miyamoto M., Nagai R., 1975, *PASJ*, **27**, 533
- Moe M., Di Stefano R., 2017, *ApJS*, **230**, 15
- Moe M., Stefano R. D., 2013, *ApJ*, **778**, 95
- Navarro J. F., Frenk C. S., White S. D. M., 1996, *ApJ*, **462**, 563
- Neunteufel P., 2020, arXiv e-prints, p. arXiv:2006.11427
- O’Connor E., Ott C. D., 2011, *ApJ*, **730**, 70
- O’Shaughnessy R., Gerosa D., Wysocki D., 2017, *Phys. Rev. Lett.*, **119**, 011101
- Oh S., Kroupa P., 2016, *A&A*, **590**, A107
- Ohlmann S. T., Röpke F. K., Pakmor R., Springel V., Müller E., 2016, *MNRAS*, **462**, L121
- Öpik E., 1924, Publications of the Tartu Astrofizika Observatory, **25**, 1
- Paczynski B., 1976, in Eggleton P., Mitton S., Whelan J., eds, IAU Symposium Vol. 73, Structure and Evolution of Close Binary Systems. p. 75
- Palladino L. E., Schlesinger K. J., Holley-Bockelmann K., Allende Prieto C., Beers T. C., Lee Y. S., Schneider D. P., 2014, *ApJ*, **780**, 7
- Perets H. B., Šubr L., 2012, *ApJ*, **751**, 133
- Perets H. B., Hopman C., Alexander T., 2007, *ApJ*, **656**, 709a–720
- Pfahl E., 2005, *ApJ*, **626**, 849
- Pfahl E., Rappaport S., Podsiadlowski P., 2002, *ApJ*, **571**, L37
- Piffl T., et al., 2014, *A&A*, **562**, A91
- Podsiadlowski P., Langer N., Poelarends A. J. T., Rappaport S., Heger A., Pfahl E., 2004, *ApJ*, **612**, 1044
- Podsiadlowski P., Ivanova N., Justham S., Rappaport S., 2010, *MNRAS*, **406**, 840
- Pols O. R., Schröder K.-P., Hurley J. R., Tout C. A., Eggleton P. P., 1998, *MNRAS*, **298**, 525
- Portegies Zwart S. F., 2000, *ApJ*, **544**, 437
- Portegies Zwart S. F., McMillan S. L. W., 2002, *ApJ*, **576**, 899
- Postnov K. A., Yungelson L. R., 2014, *Living Reviews in Relativity*, **17**, 3
- Poveda A., Ruiz J., Allen C., 1967, Boletín de los Observatorios Tonantzintla y Tacubaya, **4**, 86
- Przybilla N., Nieva M. F., Heber U., Firnstein M., Butler K., Napiwotzki R., Edelmann H., 2008a, *A&A*, **480**, L37
- Przybilla N., Fernanda Nieva M., Heber U., Butler K., 2008b, *ApJ*, **684**, L103
- Przybilla N., Nieva M.-F., Butler K., 2008c, *ApJ*, **688**, L103
- Regós E., Tout C. A., 1995, *MNRAS*, **273**, 146
- Renzo M., et al., 2019a, *MNRAS*, **482**, L102
- Renzo M., et al., 2019b, *A&A*, **624**, A66
- Repetto S., Nelemans G., 2015, *MNRAS*, **453**, 3341
- Repetto S., Davies M. B., Sigurdsson S., 2012, *MNRAS*, **425**, 2799
- Repetto S., Igoshev A. P., Nelemans G., 2017, *MNRAS*, **467**, 298
- Rossi E. M., Marchetti T., Cacciato M., Kuiack M., Sari R., 2017, *MNRAS*, **467**, 1844
- Sana H., et al., 2012, *Science*, **337**, 444
- Sana H., et al., 2013, *A&A*, **550**, A107
- Sandquist E. L., Taam R. E., Chen X., Bodenheimer P., Burkert A., 1998, *ApJ*, **500**, 909
- Schneider F. R. N., et al., 2014, *ApJ*, **780**, 117
- Schneider F. R. N., Izzard R. G., Langer N., de Mink S. E., 2015, *ApJ*, **805**, 20
- Schoettler C., Parker R. J., Arnold B., Grimmett L. P., de Bruijne J., Wright N. J., 2019, *MNRAS*, **487**, 4615
- Schoettler C., de Bruijne J., Vaher E., Parker R. J., 2020, arXiv e-prints, p. arXiv:2004.13730
- Schönrich R., Binney J., Dehnen W., 2010, *MNRAS*, **403**, 1829
- Schwab J., Podsiadlowski P., Rappaport S., 2010, *ApJ*, **719**, 722
- Sesana A., Haardt F., Madau P., 2006, *ApJ*, **651**, 392
- Sesana A., Sartore N., Devecchi B., Possenti A., 2012, *MNRAS*, **427**, 502
- Shen K. J., et al., 2018, *ApJ*, **865**, 15
- Sherwin B. D., Loeb A., O’Leary R. M., 2008, *MNRAS*, **386**, 1179
- Shklovskii I. S., 1970, Soviet Ast., **13**, 562
- Silva M. D. V., Napiwotzki R., 2011, *MNRAS*, **411**, 2596
- Snaith O. N., Haywood M., Di Matteo P., Lehnert M. D., Combes F., Katz D., Gómez A., 2014, *ApJ*, **781**, L31
- Snaith O., Haywood M., Di Matteo P., Lehnert M. D., Combes F., Katz D., Gómez A., 2015, *A&A*, **578**, A87
- Soberman G. E., Phinney E. S., van den Heuvel E. P. J., 1997, *A&A*, **327**, 620
- Socrates A., Blaes O., Hungerford A., Fryer C. L., 2005, *ApJ*, **632**, 531
- Sukhbold T., Ertl T., Woosley S. E., Brown J. M., Janka H. T., 2016, *ApJ*, **821**, 38
- Sutantyo W., 1975, *A&A*, **41**, 47
- Tauris T. M., 2015, *MNRAS*, **448**, L6
- Tauris T. M., Takens R. J., 1998, *A&A*, **330**, 1047
- Tetzlaff N., Neuhäuser R., Hohle M. M., 2011, *MNRAS*, **410**, 190
- Tillich A., Przybilla N., Scholz R.-D., Heber U., 2009, *A&A*, **507**, L37
- Tout C. A., Aarseth S. J., Pols O. R., Eggleton P. P., 1997, *MNRAS*, **291**, 732
- Uglio M., Janka H.-T., Marek A., Arcones A., 2012, *ApJ*, **757**, 69
- Vanbeveren D., Mennekens N., van den Heuvel E. P. J., Van Bever J., 2020, *A&A*, **636**, A99
- Verbunt F., Cator E., 2017, *Journal of Astrophysics and Astronomy*, **38**, 40
- Verbunt F., Igoshev A., Cator E., 2017, *A&A*, **608**, A57
- Vigna-Gómez A., et al., 2018, *MNRAS*, **481**, 4009
- Wang B., Han Z., 2009, *A&A*, **508**, L27
- Wang B., Meng X., Chen X., Han Z., 2009, *MNRAS*, **395**, 847
- Webbink R. F., 1984, *ApJ*, **277**, 355
- Webbink R. F., 2008, Common Envelope Evolution Redux. p. 233, doi:10.1007/978-1-4020-6544-6\_13
- Wheeler J. C., Lecar M., McKee C. F., 1975, *ApJ*, **200**, 145
- Willems B., Henninger M., Levin N., Ivanova N., Kalogera V., McGhee K., Timmes F. X., Fryer C. L., 2005, *ApJ*, **625**, 324

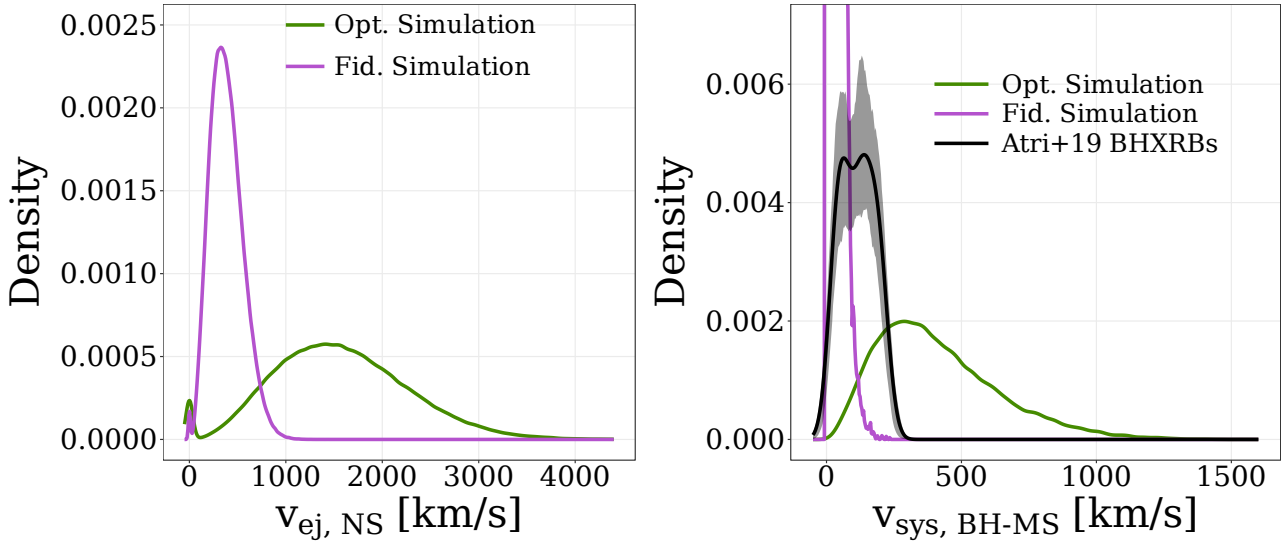


**Figure A1.** *Left:* probability-weighted ejection velocity distribution for neutron stars ejected from unbound binaries in the fiducial (violet) and optimized (green) simulations. *Right:* probability-weighted post-CC systemic velocity distributions for remaining bound black hole-main sequence binaries in the optimized (green) and fiducial (violet, cut off for visibility) simulations. Black curve shows distribution of disc-crossing velocities derived by [Atri et al. \(2019\)](#) for 16 Galactic black hole X-ray binaries. Shaded region shows  $1\sigma$  bootstrapped confidence intervals.

Williams A. A., Belokurov V., Casey A. R., Evans N. W., 2017, [MNRAS](#), **468**, 2359

Wongwathanarat A., Janka H. T., Müller E., 2013, [A&A](#), **552**, A126

Woosley S. E., 1987, in Helfand D. J., Huang J. H., eds, IAU Symposium Vol. 125, The Origin and Evolution of Neutron Stars. p. 255

Wyrzykowski L., Mandel I., 2020, [A&A](#), **636**, A20

Wyrzykowski L., et al., 2004, *Acta Astron.*, **54**, 1

Wyrzykowski L., et al., 2016, [MNRAS](#), **458**, 3012

Wysocki D., Gerosa D., O’Shaughnessy R., Belczynski K., Gladysz W., Berti E., Kesden M., Holz D. E., 2018, [Phys. Rev. D](#), **97**, 043014

Xu Y., Newberg H. J., Carlin J. L., Liu C., Deng L., Li J., Schönrich R., Yanny B., 2015, [ApJ](#), **801**, 105

Yu Q., Madau P., 2007, [MNRAS](#), **379**, 1293

Yu Q., Tremaine S., 2003, [ApJ](#), **599**, 1129

Zapartas E., et al., 2017, [ApJ](#), **842**, 125

Zhang F., Lu Y., Yu Q., 2013, [ApJ](#), **768**, 153

Zheng Z., et al., 2014, [ApJ](#), **785**, L23

Zhong J., et al., 2014, [ApJ](#), **789**, L2

Zorotovic M., Schreiber M. R., Gänsicke B. T., Nebot Gómez-Morán A., 2010, [A&A](#), **520**, A86

Zuo Z.-Y., 2015, [A&A](#), **573**, A58

Zuo Z.-Y., Li X.-D., 2014, [MNRAS](#), **442**, 1980

de Kool M., 1990, [ApJ](#), **358**, 189

de Mink S. E., Belczynski K., 2015, [ApJ](#), **814**, 58

de Mink S. E., Pols O. R., Hilditch R. W., 2007, [A&A](#), **467**, 1181

de Mink S. E., Brott I., Cantiello M., Izzard R. G., Langer N., Sana H., 2012, Challenges for Understanding the Evolution of Massive Stars: Rotation, Binarity, and Mergers. p. 65

de Mink S. E., Langer N., Izzard R. G., Sana H., de Koter A., 2013, [ApJ](#), **764**, 166

van Oijen J. G. J., 1989, [A&A](#), **217**, 115

van den Heuvel E. P. J., Portegies Zwart S. F., de Mink S. E., 2017, [MNRAS](#), **471**, 4256

## APPENDIX A: KINEMATICS OF UNBOUND NEUTRON STARS AND BOUND BLACK HOLE X-RAY BINARIES

Fig. A1 shows velocity distributions for both neutron stars ejected from unbound binaries (left) and systemic velocities of black hole X-ray binaries which remain bound post-CC. Distributions are shown for both the fiducial and optimized simulations. See Sec. 5.2 for more details.

This paper has been typeset from a  $\text{\LaTeX}$  file prepared by the author.